

TABLE OF CONTENTS

Acknowledgments	v
List of Tables	vii
List of Figures	viii
Chapter 1: Introduction and Background	1
1.1 Global warming and role of transport section emissions	1
1.2 Current transportation scenario	3
1.3 Evolution in internal combustion engines technology and efficiency .	4
1.3.1 Improvements on overall engine efficiency in the last decades	4
1.3.2 Emission limitations and trends in nowadays technology improvement .	6
1.3.3 The importance of waste heat recovery	9
1.4 Objectives and structure of the thesis	11
Chapter 2: Review of the state of the art	12
2.1 Introduction to bottoming recuperative cycles	12
2.1.1 Steam Rankine cycle	12
2.1.2 Organic Rankine cycle	13
2.1.3 Brayton cycle	15
2.1.4 Selection of the bottoming cycle	16
2.2 Introduction to split cycle engines	18

2.2.1	Basic principles	18
2.2.2	Split-cycle engine operation	20
2.2.3	Intra-cycle Waste Heat Recovery	21
Chapter 3: Modeling		23
3.1	Introduction to the model	23
3.1.1	Inputs and outputs	23
3.1.2	Forward and backward modeling approach	24
3.2	Equations for the mechanical behavior	24
3.2.1	Vehicle Longitudinal Dynamics Model	25
3.2.2	Transmission model	25
3.2.3	Torque converter model	26
3.3	Energy balance	26
3.3.1	Thermal model	27
3.3.2	Radiator model	29
3.3.3	Coolant flow and engine heat rejection model	29
3.4	Results	29
References		36

LIST OF TABLES

1.1	1 st and 2 nd law of thermodynamics fuel energy and exergy distributions	10
1.2	Research results on waste heat recovery benefits	11
3.1	Inputs and outputs of the engine model	24

LIST OF FIGURES

1.1	Global mean temperature estiamates based on land and ocean data[2]	1
1.2	Antropogenic GHG emissions by group of gases (1970 - 2010) [1]	2
1.3	Review of different mitigation scenarios for 450 ppm	2
1.4	Radiative forcing due to 2000 level emissions grouped by sector in a) 2020 and b) 2100	3
1.5	Average fuel efficiency for U.S. vehicles	4
1.6	Adjusted CO ₂ and fuel economy for vehicles model year from 1975 to 2016	5
1.7	Trends of fuel consumption variation with the introduction of major fuel delivery and valve-train control technologies	6
1.8	Percentage of MY equipped with a certain technology	7
1.9	Comparison of emissions standards with reference to Euro standards	7
1.10	Emissions limits for a) Gasoline and b) Diesel light vehicles in USA and Europe	8
1.11	Distribution of Gasoline Turbo Vehicles by Displacement and Horse-power, MY 2010, 2013, and 2016	8
1.12	Comparison fuel economy between non hybrid and hybrid cars and hybrid cars production	9
1.13	Typical energy balance of a Euro 6 diesel engine	10
2.1	Bottoming cycle	12
2.2	Steam Rankine cycle T-s diagram and physical layout	13
2.3	T-s diagram and plant layout for a generic Organic Rankine Cycle . .	14

2.4	Comparison of different Rankine Cycle working fluid characteristics	15
2.5	Different ORC layouts: structure 1, 2 and 3	15
2.6	Diagrams and plant layout of an idealized Brayton cycle	16
2.7	Simplest plant layout for a split cycle engine	19
2.8	Valve events for SSC engine at 4000 RPM and full load conditions . .	20
2.9	a) Comparison of the energy fluxes between an intra-cycle waste recovery and bottoming cycle type recovery, b) T-s and p-crank angle diagram for a split cycle engine with ICWHR	21
2.10	Schematic of the engine equipped with quasi-isothermal compression and ICWHR	22
3.1	Block diagram of the model	23
3.2	Block diagram of Powertrain Forward-Looking and Backward-Looking Model	25
3.3	Maps for the unlocked torque converter	26
3.4	Block diagram of the thermal system model	26
3.5	Three mass engine model and general engine division into parts . . .	27
3.6	Energy flows in the engines	28
3.7	Speed profiles of the considered drivecycles	30
3.8	Lockup and gear profiles	30
3.9	Rotational speed at transmission input	31
3.10	Rotational speed at the engine	31
3.11	Engine torque	31
3.12	Fuel mass flow rate	32
3.13	Thermostat position and fan speed	32
3.14	Temperatures of engine fluids	33

CHAPTER 1

INTRODUCTION AND BACKGROUND

The focus on reduction of greenhouse emissions from fossil fuels is today as important as ever. The rapid ongoing modifications of climate conditions are raising concerns and awareness in this regard. Total anthropogenic greenhouse emissions have continued to increase over 1970 to 2010, with larger absolute increase per decade toward the end of this period, with CO₂ emissions from fossil fuel combustion and industrial processes contributing about 78% of the total. Annual anthropogenic GHG emissions have increased by 10 Gtons equivalent of CO₂ between 2000 and 2010, with this increase directly coming from energy supply (47%), industry (30%), transport (11%) and buildings (3%) sectors [1].

Global warming causes adverse effect and mutations on natural habitats and natural equilibriums of Earth, and is held responsible for increase of atmospheric temperature, acidification of oceans, melting of the permafrost, increased frequency of extreme weather events and others. As a result, many species struggle to adapt to these new environmental conditions and some are facing extinction. Even human related activities are in danger, as the natural habitat become more and more hostile to plants and animals. In the following sections the phenomenon will be explained in more details, and the role of transportation sector will be highlighted.

1.1 Global warming and role of transport section emissions

Global warming and *Climate change* are terms used for describing the increase in surface and ocean temperature registered in the last century. Due to the accumulation of greenhouse gases, additional energy is stored in the atmosphere and the oceans, causing ice melting and warming of continents and atmosphere.

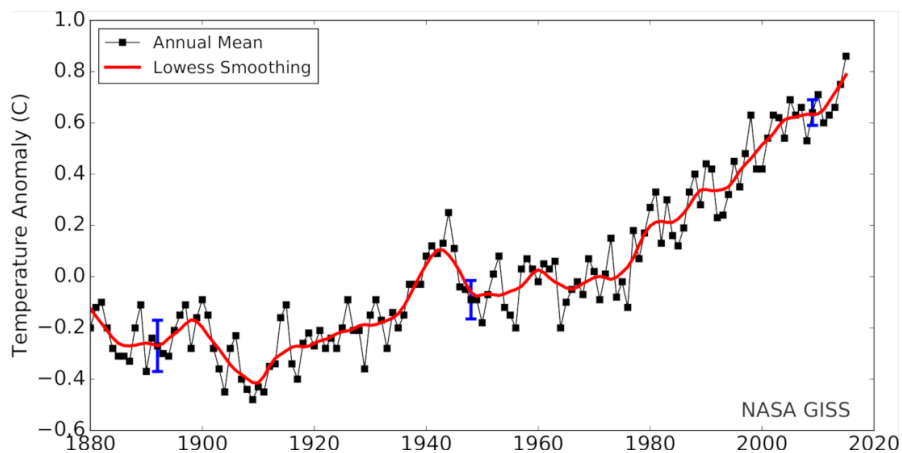


Figure 1.1: Global mean temperature estimates based on land and ocean data[2]

Without additional efforts to reduce GHG emissions beyond those in place today, emissions growth is expected to persist driven by growth in global population and economic activities. Baseline scenarios, those without additional mitigation, result in global mean surface temperature increases in 2100 from 3.7 °C to 4.8 °C compared

to pre-industrial levels [1]. Of the 49 Gt CO₂,eq emitted in 2010, the *transportation* sector is responsible for 14.3% of the total, ranking as the fourth major emitter economic sector after Electricity and Heat production, Agriculture and Land use, and Industry.

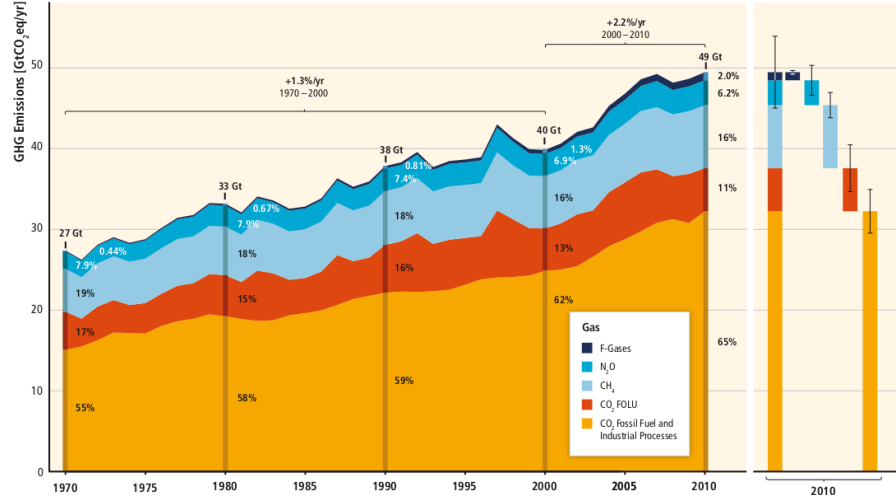


Figure 1.2: Anthropogenic GHG emissions by group of gases (1970 - 2010) [1]

The scientific community mainly agrees on trying to keep the temperature increase with respect to pre-industrial levels under 2°C, equivalent to atmospheric concentrations in 2100 of about 450 ppm CO₂,eq. The aforementioned scenarios include substantial cuts in anthropogenic GHG emissions by mid century through large scale changes in energy systems and potentially land use. Scenarios reaching these concentrations by 2100 are characterized by lower global GHG emissions in 2050 than in 2010, 40% to 70% lower globally, and emissions levels near zero Gt CO₂,eq or below in 2100 [1]. In Figure 1.3, the reduction in emissions for the major economic sectors is reported. It's possible to notice how, especially in the case without heavy implementation of carbon dioxide capture plants, the amount of greenhouse gases released in the atmosphere by transport must be greatly reduced.

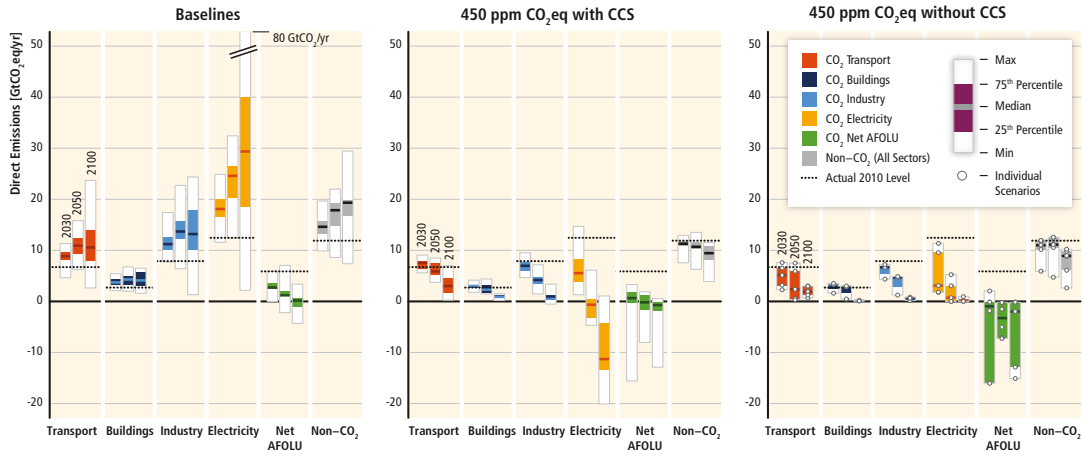


Figure 1.3: Review of different mitigation scenarios for 450 ppm

The chart represents a review of the major models and scenarios available to date, and taken into consideration in [1]. According to the same study, efficiency en-

hancements and behavioural changes aimed at reducing energy demand compared to baseline scenarios without compromising development, are a key mitigation strategy in scenarios reaching atmospheric CO_{2,eq} concentrations of about 450 to about 500 ppm by 2100.

The transport sector accounted for 27% of final energy use and 6.7 Gt CO₂ direct emissions in 2010, with baseline CO₂ emissions projected to approximately double by 2050. Technical and behavioural mitigation measures for all transport modes, plus new infrastructure and urban redevelopment investments, could reduce final energy demand in 2050 by around 40% below the baseline [1].

A study by Unger and al.[3] attributes a radiative forcing value to different economic sectors that are the main emitters in today economy. The radiative forcing concept has been developed in order to quantify the human and natural influence on the climate system, and is defined as the net energy flux difference at the top of the atmosphere. In Figure1.4, the positive and negative contributions of the different economic sectors are presented. It's important to notice how on-road transportation is foreseen to be the major responsible for increasing of atmospheric energy content in 2020, and the second most important factor in 2100. This is due to the peculiar composition of exhaust gases produced by vehicles: the production is mainly constituted by components that contribute to trapping heat. Other sectors, as the power sector, produce much more components that trap heat, but the net contribution is reduced by the amount of components as black-carbon, that reflects the solar radiation and contribute to cooling down the atmosphere.

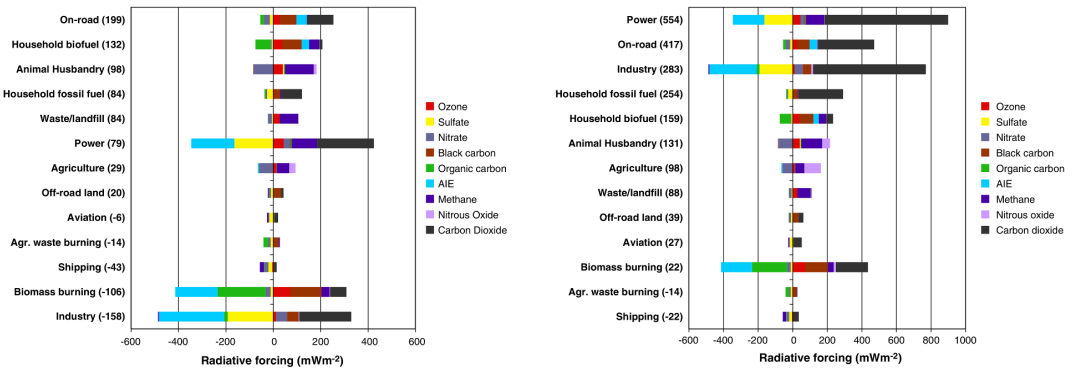


Figure1.4: Radiative forcing due to 2000 level emissions grouped by sector in a) 2020 and b) 2100

1.2 Current transportation scenario

The average efficiency of modern internal combustion engines is measured to be around 32% - 36% for Diesel engines, and around 29% - 32% for Gasoline engines.

According to the evidence reported in section1.1, being the transportation sector one of the main culprits for global warming, an increase in efficiency of passenger vehicles can play an important role in mitigating climate change. Figure1.5 shows how, in the 1980 - 2014 considered timeframe, the specific fuel consumption of U.S. vehicles has been reduced thanks to technical advancements[4].

Taking a more in depth look at the emissions figure of the transportation economy itself, when considering the energy use by transportation mode in 2013, High-

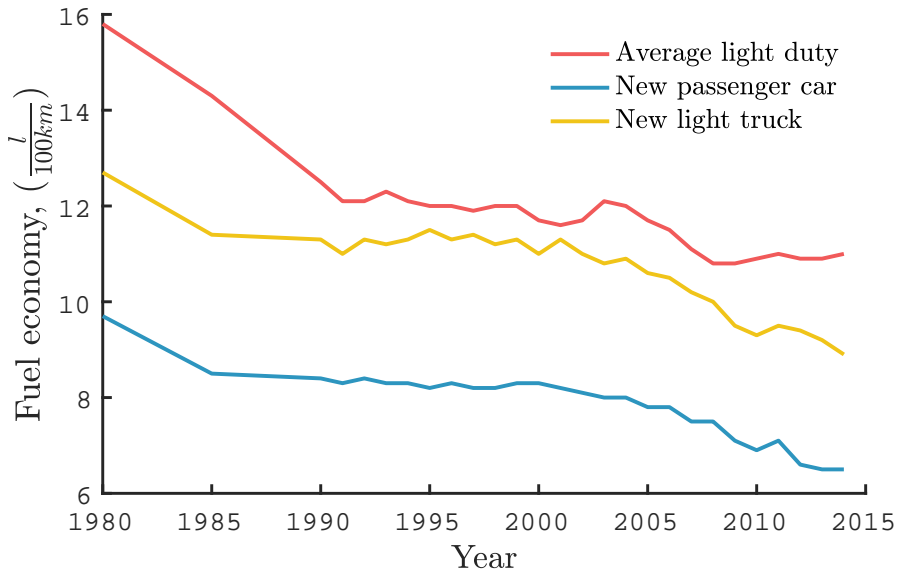


Figure 1.5: Average fuel efficiency for U.S. vehicles

wway is by far the sector that consumes the greater share of the total (83.2%), followed by Air transportation (6.9%) and Water transportation (3.9%). The Highway energy usage can be once again split between Light-duty (52.2%), Combination Truck (15.3%), Single-unit truck (7.6%), and Bus (1.1%). Certified air carriers experienced the largest total decrease in fuel consumption, consuming about 3.6 billion fewer gallons of jet fuel in 2014 than in 2000. General aviation gasoline showed the largest percent decrease in fuel consumption from 2000 to 2014, declining by 40.8 percent. Additionally, water modes powered by residual fuel oil also showed a large decrease, declining by nearly 2.6 billion gallons during the same period. Consistent with increases in vehicle-miles traveled, light-duty highway vehicles used about 430 million more gallons of gasoline in 2014 than in 2000[5].

According to the evidence shown, the amount of effort spent on researching and experimenting new and more advanced ways of reducing transportation energy consumption is justified. Numerous different technical trends are nowadays gaining traction in the automotive field, such as downsizing and turbocharging of gasoline engines, or the usage of different cycles. A more in depth analysis will be provided in Section 1.3.2.

1.3 Evolution in internal combustion engines technology and efficiency

In this section a review of the key technical improvements occurred to internal combustion engines in the last decades is presented, among with a brief explanation of the current emission limitation rules for both the USA and Europe. The final section will cover the importance of *Waste Heat Recovery* (WHR) and why it needs to be researched and adopted in the next years in order to achieve the planned emissions limitation objectives.

1.3.1 Improvements on overall engine efficiency in the last decades

Since the petroleum crysis of the '70s, an increasing effort on reduction of fuel consumption and increase of power density has begun.

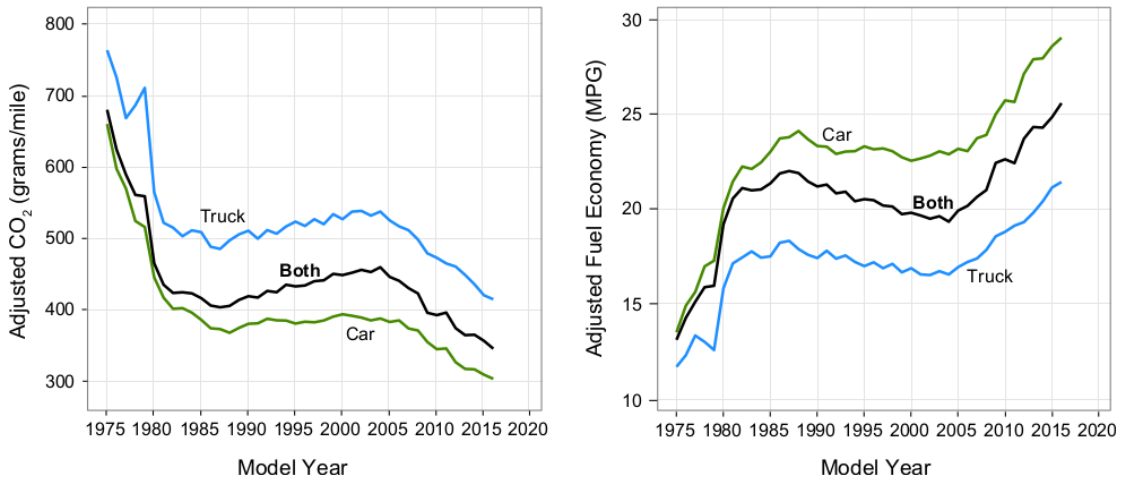


Figure1.6: Adjusted CO₂ and fuel economy for vehicles model year from 1975 to 2016

As shown in Figure1.6[6], during the last four decades, the fuel consumption and carbon dioxide emissions has been vastly reduced. This great improvement has been possible thanks to some key technical turning points.

One of the main design aspects that have changed significantly over time is how the fuel is delivered into the engine. Until the early 1980s the majority of engines used carburetors to meter fuel delivered to the combustion chamber. More recently, engines with gasoline direct injection (GDI) have begun to replace engines with port fuel injection. GDI equipped engines were first introduced with very limited production in Model Year (MY) 2007. Eight years later GDI engines were installed in about 42% of MY 2015 vehicles, and are projected to achieve a 49% market share in MY 2016[6].

Another key aspect of engine design that has been vastly improved is the valve-train. The number of valves per cylinder and the ability to alter valve timing during the combustion cycle allowed significant power and efficiency improvements, as nowadays almost the entire fleet of the most relevant car manufacturers has converted to multi-valve design. While some three and five valve engines have been produced, the vast majority of multi-valve engines are based on four valves per cylinder[6]. In addition to the number of valves per cylinder, designs have evolved that allow engine valves to vary the timing when they are opened or closed with respect to the combustion cycle, creating more flexibility to control engine efficiency, power, and emissions. In Figure1.7, the fuel consumption reduction made possible by the improved valve-train and fuel delivery is shown.

As a result of the new fuel delivery systems, along with other reasons, two very noticeable trends in horsepower and displacement delineated. Average horsepower climbed consistently from MY 1982 to MY 2008. Since MY 2008, horsepower trends have been less consistent, and may be beginning to flatten out. From MY 1975 to 1987, the average engine displacement of new vehicles dropped dramatically by nearly 40 %. From MY 1988 to 2004, displacement generally grew slowly, but the trend reversed in 2005 and engine displacement has been generally decreasing since. In MY 2016, engine displacement is projected to reach the lowest point on record, below the previous lowest average displacement reached in MY 1987[6].

The contrasting trends in horsepower increase and displacement decrease are a

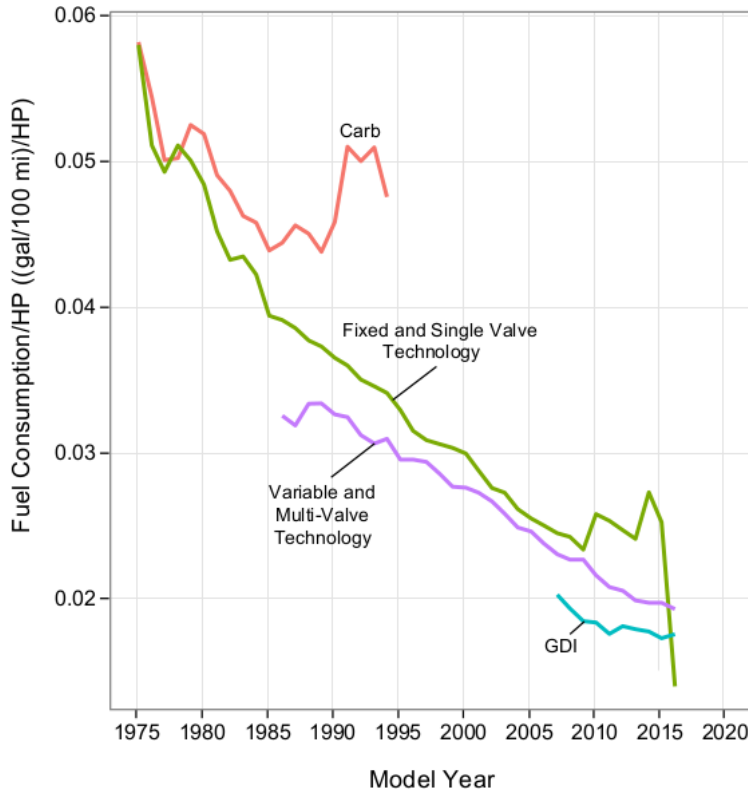


Figure1.7: Trends of fuel consumption variation with the introduction of major fuel delivery and valve-train control technologies

proof of the continued improvements in engine design and of the impact of new technologies. The final result is a steady quasi-linear increase of the power density from around $0.5 \frac{HP}{Displacement}$ in 1975 to around $1.4 \frac{HP}{Displacement}$ in 2016, with a growth rate of $0.02 \frac{HP}{in^2 \cdot year}$. Also the average number of cylinders has gradually reduced.

In Figure1.8, a summary of the time trends of the major innovations is reported.

1.3.2 Emission limitations and trends in nowadays technology improvement

Emission limitations are among the main drivers that fostered the continuous strive of greater efficiency in internal combustion engines. In Figure1.9 a review of the most important emissions standards from across the world, and their Euro equivalence is presented[7]. In Figure1.10 are reported the emission limits for gasoline and diesel powered light vehicles in both USA and Europe[8].

In order to respect the emission standards imposed by current and future rules, the major car manufacturers are adopting new technologies, and some trends are delineating.

Probably the most noticeable trend in new engines is the *turbo-downsizing*. This new group of engines is characterized usually by a similar power output with respect to the engine that are replacing, but a smaller displacement. This result is achieved by the introduction of turbochargers and, often but not always, GDI. Turbo downsized engines are an approach to engine design that provides increased fuel economy by using a smaller engine for most vehicle operation, while retaining the ability to provide more power via the turbocharger, when needed. Turbocharged engines are

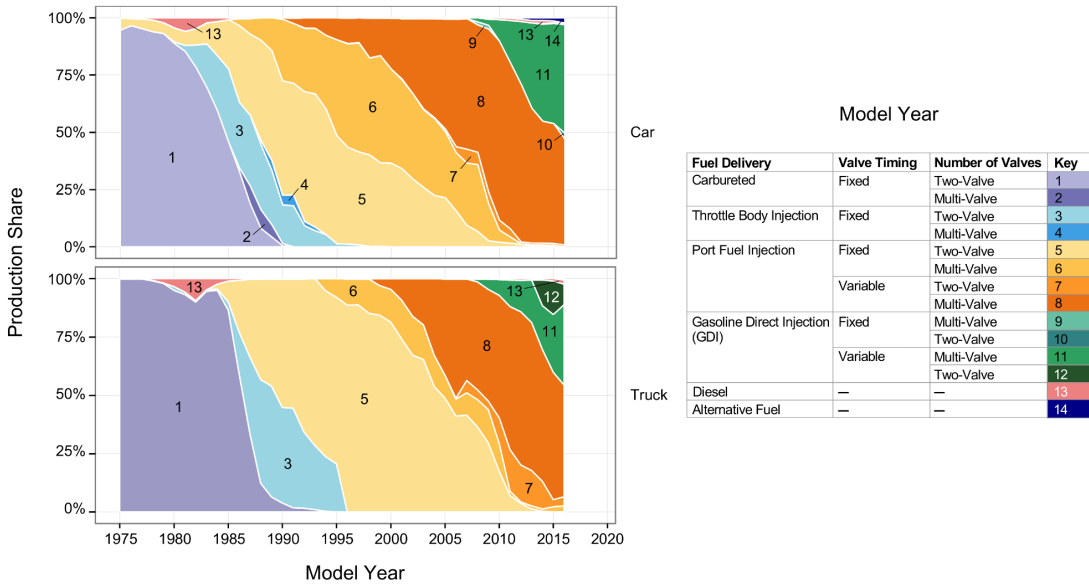


Figure 1.8: Percentage of MY equipped with a certain technology

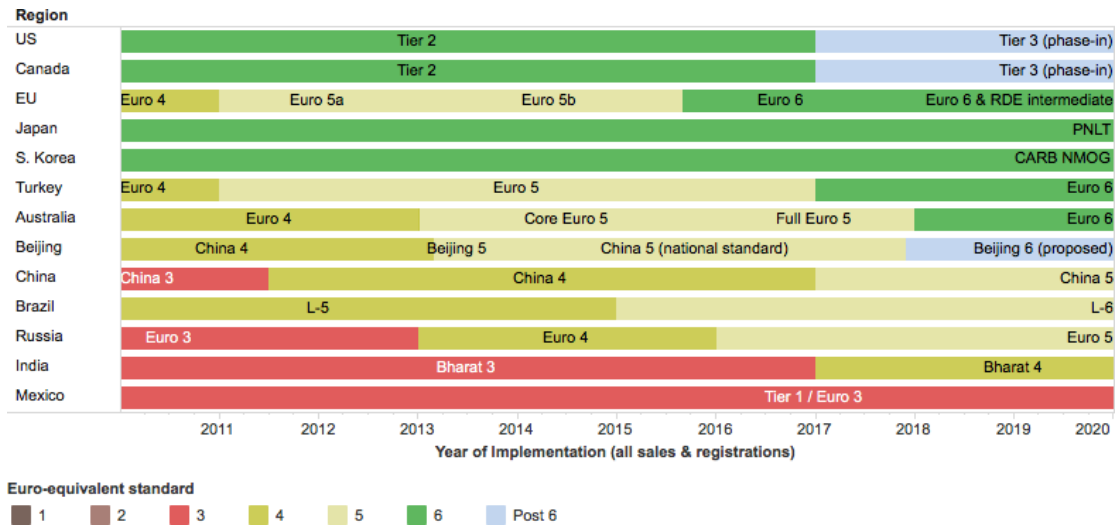


Figure 1.9: Comparison of emissions standards with reference to Euro standards

projected to constitute 22% of new vehicle production in 2016, and the penetration trend appears to increase rapidly[6]. This is due to the fact the traditionally turbocharged engines were mainly used in high performance vehicles, while now they are being used also on mainstream vehicles. The increased power density and torque made available by the adoption of the turbocharger allows the shifting to designs with fewer cylinders, while the combination with GDI allows a more efficient engine operation and increases the resistance to knocking. In MY 2016, more than 90% of new vehicles with gasoline turbocharged engines also use GDI[6]. In Figure 1.11, the distribution of gasoline turbo vehicles is shown. Other new technologies that are gaining traction in the engine design environment are Cylinder Deactivation, Non-Hybrid Stop/Start, and more advanced transmissions, both in form of transmissions with seven or more gears or Continuous-Variable Transmissions (CVT).

Hybrid vehicle technology is the most diffused technique used to increase the fuel efficiency in ways that transcend the pure ICE efficiency increase. Hybrid vehicles

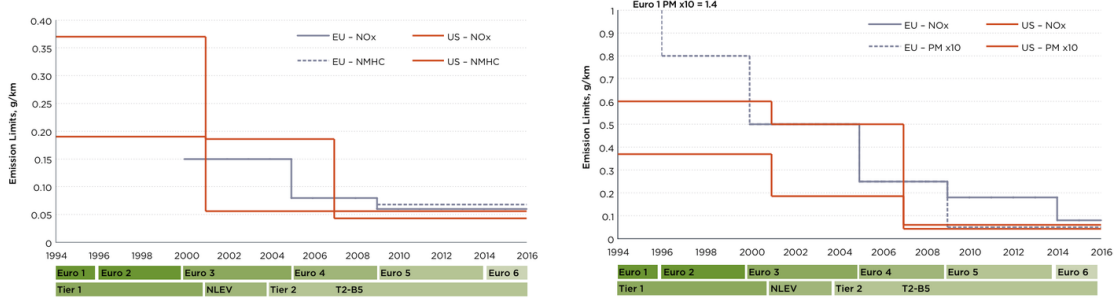


Figure 1.10: Emissions limits for a) Gasoline and b) Diesel light vehicles in USA and Europe

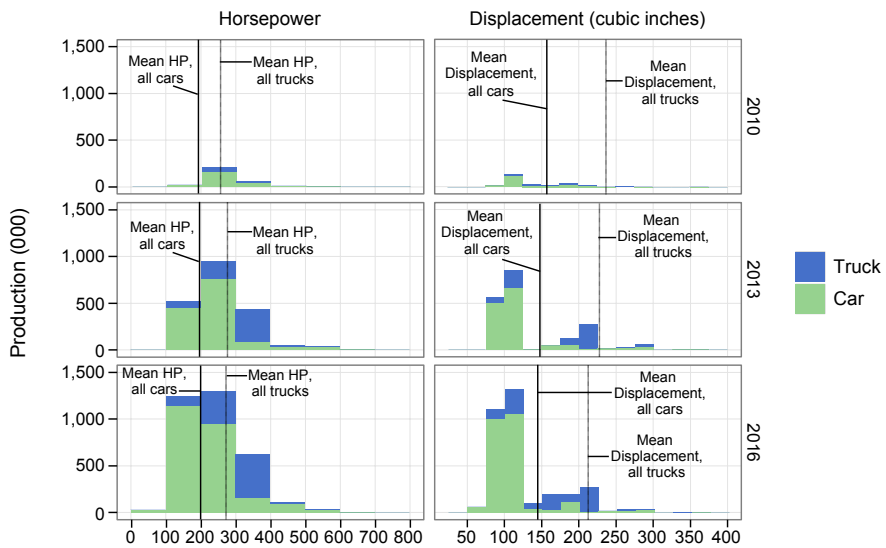


Figure 1.11: Distribution of Gasoline Turbo Vehicles by Displacement and Horsepower, MY 2010, 2013, and 2016

utilize larger battery packs, electric motors, and other components that can increase vehicle fuel economy. Benefits of hybrids include:

- regenerative braking which can capture energy that is otherwise lost in conventional friction braking to charge the battery
- availability of two sources of on-board power which can allow the engine to be operated at or near its peak efficiency more often
- shutting off the engine at idle.

Most hybrids provide higher fuel economy than comparable vehicles, although some hybrids have been offered as more performance-oriented vehicles with more minor fuel economy improvements. In Figure 1.12 it's shown the distribution in time of the fuel economy between hybrid and non hybrid vehicles, and the historical production of hybrid and electric vehicles.

While the average fuel economy of hybrid cars remains higher than the average fuel economy of non-hybrid cars, the difference appears to be narrowing. Average hybrid car fuel economy has been relatively stable since MY 2001, while the fuel economy of the average non-hybrid car has increased more than 27%. Since MY

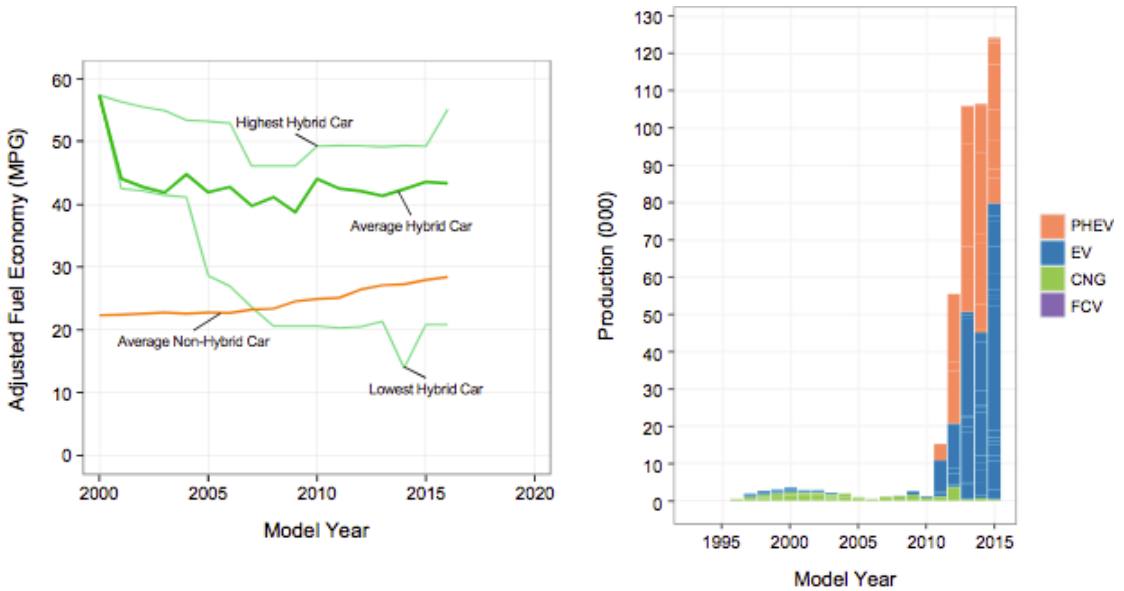


Figure 1.12: Comparison fuel economy between non hybrid and hybrid cars and hybrid cars production

2004, the difference in fuel economy between the average hybrid midsize car and the average non-hybrid midsize gasoline car has narrowed from about 25 mpg to about 14 mpg. The primary reason for this trend is continued improvements to the internal combustion engine. Additionally, many technologies introduced or emphasized in early hybrids, such as improved aerodynamics, low rolling resistance tires, and increased use of lightweight materials, have also become more common on non-hybrid vehicles[6].

1.3.3 The importance of waste heat recovery

In the previous sections a brief review of how some of the key technical improvements have modified engine design, performances and fuel consumption have been provided.

One of the main causes of the relatively low efficiency of even modern ICEs is that a significant amount of energy produced by fuel combustion is wasted in form of heat, then not used to produce useful power. In internal combustion engines, only a small part of the fuel energy flow is transformed into power available at the crankshaft. For the best points of operation, diesel engines have a maximum efficiency approaching 45% while gasoline engines have efficiencies of about 35%. For both engines, the most part of the fuel energy flow is therefore lost as coolant heat flow and exhaust gases heat flow. In everyday operating conditions, cars have average engine efficiencies on driving cycles well below their top values, with the heat flow lost in the exhaust gases and the engine coolant increasing accordingly. In many driving conditions, the waste heat flow represents an important part of the fuel energy flow. The energy flow potentially available to be converted to usable power in the exhaust gases and the coolant is therefore quite significant[9]. Considering the large number of vehicles in the world, such waste energy makes great impact to our environment globally.

It has been estimated that the thermal efficiency of a modern IC engine is limited to 20 - 40% while 33% of the fuel energy from a typical medium-size passenger vehicle

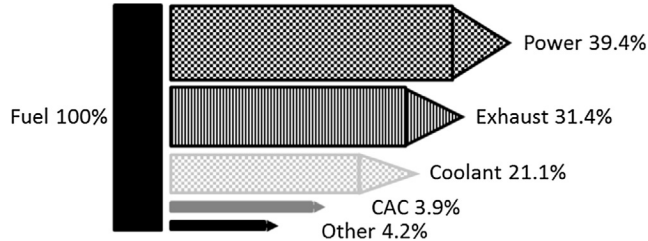


Figure 1.13: Typical energy balance of a Euro 6 diesel engine

	1st law	2nd law
Brake work	10.4%	9.7%
Exhaust	27.7%	8.4%
Irreversibilities, Friction, Coolant, and other	61.9%	81.9%

Table 1.1: 1st and 2nd law of thermodynamics fuel energy and exergy distributions

is carried away by exhaust gases and 29% is carried away by engine cooling water in urban traffic conditions. Depending on engine type and operating conditions, the IC exhaust gas temperature usually varies from 500 to 900 °C and engine cooling water temperature is around 100 °C. It is reported that for a typical light duty 4 cylinder spark ignition engine, the waste energy carried by the exhaust gas ranges from 4.6 to 120 kW and cooling water heat ranges from 9 to 48 kW [10], which makes the exhaust gas and engine cooling heat very attractive for energy recovery. It's possible to harvest part of this waste energy from vehicles and produce regenerated mechanical or electrical power.

According to [11], experimental data coming from a series of tests on a turbocharged 2007 Saab vehicle shows engine-out exhaust temperature from 400 to 600 °C. The exhaust temperature range of naturally aspirated gasoline engine is higher, typically from 450 to 800 °C. The same research performed a FTP-75 test cycle with the aforementioned vehicle, and measured that the total fuel energy consumed during the course of the driving cycle is approximately 58.5 MJ, or about 1.7 L of unleaded gasoline fuel. The percentage of fuel energy converted to useful work for this driving cycle (i.e. the vehicle thermal efficiency) is 10.4%. A much larger portion of fuel energy, 27.7%, exits the vehicle in the form of thermal energy in the exhaust, while the remaining 61.9% of the energy balance consists of energy losses to friction, coolant, and other. Only a portion of the energy in the exhaust is available for recovery due to process irreversibilities, ambient conditions, or other.

In Table 1.1 are reported the energy and exergy distributions with respect of the fuel entering the engine. It's possible to notice how, according to the 2nd law of thermodynamics, the exhaust exergy is nearly as high as the amount of brake work. Thus, there is an abundant amount of available energy present in the exhaust of modern gasoline vehicles that can be used to improve overall system efficiency if an effective means of energy recovery can be employed. In another research [12] the value of exhaust gases mentioned to be 18.6% of total combustion energy. It is also found that by installing heat exchanger to recover exhaust energy of the engine could be saved up to 34% of fuel saving [13].

Many studies highlighted the validity of the idea of recovering this waste heat to

Reference	Year	Vehicle	Heat Source	Research method	$\Delta\eta_{th}$	$\Delta\eta_{mec}$
[14]	1993	Passenger car	Coolant	Experiment	/	3%
[10]	2005	HEV	Exhaust	Numerical	1.3-5%	/
[15]	2006	Prius	Exhaust + engine block	Numerical	5.50%	/
[16, 17]	2007	HEV	Exhaust	Experiment	3.80%	/
[18]	2008	3 series	Exhaust + Coolant	Experiment	5.70%	/
[19]	2009	HEV-Prius	Exhaust + Coolant	Numerical	/	9%
[20, 21]	2011	Toyota 8A-FE	Exhaust, Lubricant, Coolant	Experiment	12-17.3%	/
[22, 23]	2012	5 series	Exhaust	Experiment	/	6%
[9, 24]	2012	1.8L engine	Exhaust + Coolant	Numerical	1.7-5.1%	/
[25]	2012	BL18T engine	Exhaust + Coolant	Numerical	3-6%	/
[26]	2013	2.8L VR6	Exhaust	Experiment	/	2.64-6.96%

Table1.2: Research results on waste heat recovery benefits

produce additional power, and the research and actual production efforts showed promising results. In Table1.2 are listed some of the most relevant research and production vehicles equipped with a waste heat recovery system, among with the achieved increase in thermal and mechanical efficiency.

1.4 Objectives and structure of the thesis

The main objective of the thesis is to compare three different technologies that aim at recovering waste heat produced by the internal combustion engine. In particular, two different *Organic Rankine bottoming Cycles* (ORC) paired with an Otto-cycle engine, and a *Split-Cycle Engine* with *isothermal compression* and *integrated waste heat recovery*.

The comparison will be performed via MATLAB/Simulink simulations. A backward-looking model will take as input the velocity profile of a driving cycle for which experimental data is available, then the torque and angular speed at the engine will be calculated through a simulated transmission. Furthermore, engine maps will be extracted from experimental data along with characteristics and performances of the heat exchangers, making possible the calculation of flow rate, temperature and heat flux for both the exhaust gases and the coolant. Once the waste heat data will be available, the bottoming cycle model will be introduced. Starting from the output of the powertrain model, the recovered energy and produced power will be calculated.

*ADD METHODOLOGIES MODEL SPLIT-CYCLE
TO BE CONTINUED WITH STRUCTURE*

CHAPTER 2

REVIEW OF THE STATE OF THE ART

2.1 Introduction to bottoming recuperative cycles

A bottoming cycle is a waste-heat recovery thermodynamic cycle that recaptures the unused energy and uses it to produce steam to drive a steam turbine generator to produce additional energy. In Figure 2.1 is shown a general configuration for a bottoming cycle. In the passenger case car, the thermal process upstream the cycle is the internal combustion engine itself.

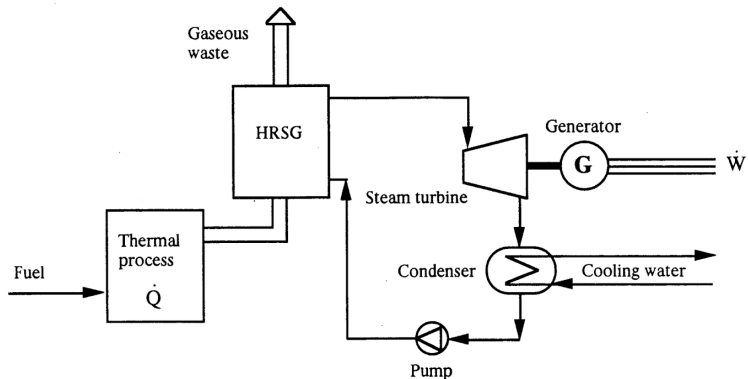


Figure 2.1: Bottoming cycle

A bottoming cycle is a powerful mean to recover the waste heat produced by an automotive internal combustion engine, and the additional power produced can be employed in different ways. It is possible to produce additional mechanical work, increasing the torque at the shaft, or produce electrical work that can be employed in different ways. Usually the selected recovery strategy is to use the recuperative cycle to produce mechanical power: this implementation is simpler and effective, but fails to achieve the maximum potential with respect to the operative conditions of the additional cycle. In this configuration the angular speed of the turbine is the same as the one of the shaft, but this speed can be different from the one of maximum efficiency of the turbo-machine.

The configuration that converts the additional power in electrical power can solve this issue. Being the system no more coupled with the shaft of the internal combustion engine but with an electric generator, the rotational speed of the turbine can be varied at will in order to achieve the most efficient operative point. The electricity produced can be stored in batteries if they are available (i.e. Hybrid or Plug-in vehicle), or used to power up auxiliaries and reduce the alternator load on the engine.

In the following sections a brief overview of the most common thermodynamic cycles that can be used as a recuperative bottoming cycle will be provided.

2.1.1 Steam Rankine cycle

The steam Rankine cycle is one of the most famous and used thermodynamic cycles for producing power. In this cycle the heat is provided externally to a closed loop,

in which water flows as a working fluid. The efficiency of the Rankine cycle can be calculated as:

$$\eta_t = \frac{\dot{W}_{thermal} - \dot{W}}{\dot{Q}_{in}} \approx \frac{\dot{W}_{turb}}{\dot{Q}_{in}} \quad (2.1)$$

This type of cycle is commonly used in thermal power generation plants. The efficiency of the Rankine cycle is limited by the high heat of vaporization of the working fluid. Also, unless the pressure and temperature reach super critical levels in the steam boiler, the temperature range the cycle can operate over is quite small: steam turbine entry temperatures are typically around 565 °C and steam condenser temperatures are around 30 °C.

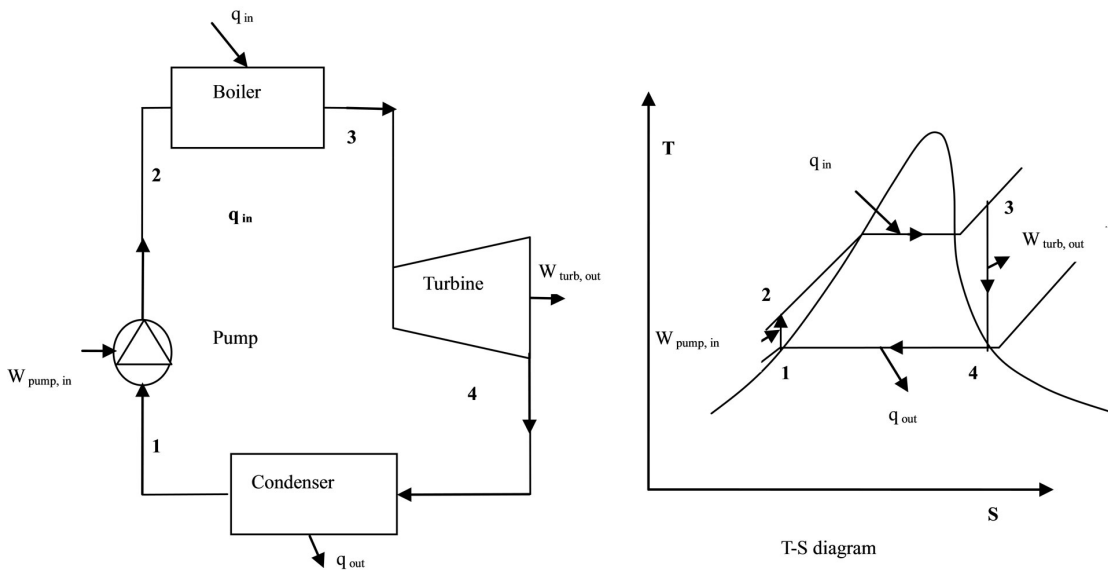


Figure 2.2: Steam Rankine cycle T-s diagram and physical layout

The process is composed by four consecutive processes, as shown in Figure 2.2:

- **Process 1-2:** the working fluid is pumped from low to high pressure. Since the fluid is in liquid form, the work required for pumping is small.
- **Process 2-3:** the liquid at high pressure is heated at almost constant pressure by an external source until it becomes dry saturated vapor.
- **Process 3-4:** the dry saturated vapor is expanded through a turbine, hence generating power. The working fluid experience a decrease of pressure and temperature, with possible partial condensation.
- **Process 4-1:** the wet vapor enters the condenser and returns to saturated liquid conditions.

2.1.2 Organic Rankine cycle

The Organic Rankine Cycle (ORC) is a particular use case of a Rankine thermodynamic cycle. It's named for its use of an organic, high molecular mass fluid with a liquid-vapor phase change, or boiling point, occurring at a lower temperature than

the water-steam phase change. The fluid allows Rankine cycle heat recovery from lower temperature sources such as coolant from internal combustion engines. The low-grade waste heat is converted into useful work, that can itself be converted into mechanical or electrical power. In Figure 2.3, the T-s diagram and the plant layout for a generic Organic Rankine Cycle are shown. The formulation of the efficiency is the same as the Steam Rankine Cycle, shown in Equation 2.1.

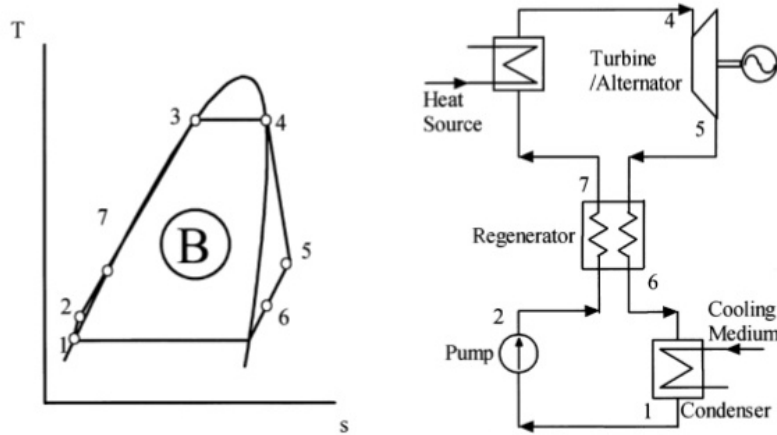


Figure 2.3: T-s diagram and plant layout for a generic Organic Rankine Cycle

The system itself is made of four components: evaporator, expander, condenser and pump. Usually a recuperator is also used, to increase the efficiency and hence the production of useful power. The waste heat is used in the evaporator to vaporize the working fluid and convert the heat in mechanical work in the expander.

The selection of the working fluid is of key importance in low temperature Rankine Cycles. Because of the low temperature, heat transfer inefficiencies have a major importance. In order to recover low-grade heat, the fluid generally has a lower boiling temperature than water, then refrigerants and hydrocarbons are two commonly used components. Water is a preferable working fluid for high exhaust gas temperatures ranging from 500 °C to 800 °C, while refrigerants are better suited for lower temperatures, as in the gas of the exhaust gases. Water also has the disadvantage that requires superheating to avoid turbine blade erosion, but the high degree of superheating makes it less practical for automotive application due to the variation of exhaust temperature at different load conditions. In figure 2.4 are reported the different T-s diagram related to different Rankine cycle working fluids.

In current years, an increasing environmental awareness has provoked the shifting from traditional refrigerants (i.e. R134a, R236fa, R245fa) to new refrigerants, characterized by lower harm potential to passengers in case of leakage or crashes, and a lower flammability level (i.e. R1233zd, R1234yf).

When considering an ORC coupled with an internal combustion engine, different possible configurations must be considered. The most common and simple structure utilizes the exhaust gas as the only heat source to evaporate the working fluid. The second structure adds another heat exchanger (recuperator) before the evaporator, using the steam from the expander to preheat the working fluid. A third structure uses waste heat from engine coolant to preheat the working fluid. The regenerative preheating of structure 2 requires a very complex liquid-gas heat exchanger with high exchange surfaces, while the preheater in structure 3 only requires a simple liquid-

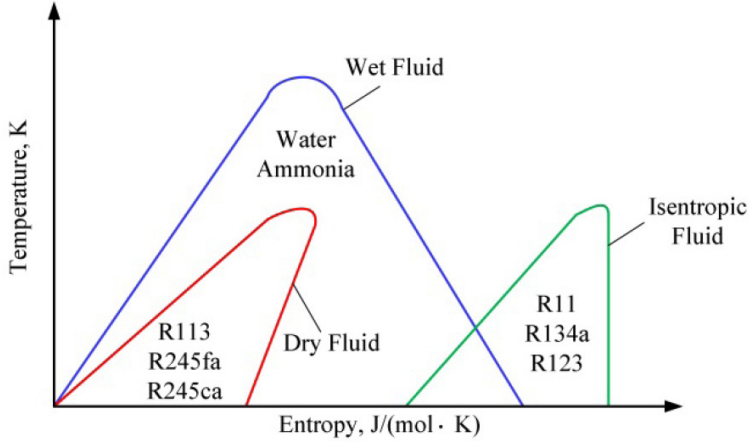


Figure 2.4: Comparison of different Rankine Cycle working fluid characteristics

liquid heat exchanger. There have been contradicting conclusions about the effect of preheating using engine coolant on the RC system efficiency. Based on Vaja and Gambarotta's work [27], the RC system with a preheater allows a net increase in power output, compared to structure 1, of 10% to 35%, depending on which working fluid is chosen. Alberto Boretti [9] also showed a 8.2% fuel economy improvement using engine coolant to preheat the RC cycle, compared to a 6.4% improvement when only exhaust gas is used to boil the working fluid. Arias et al. [15] also compared the combined exhaust and engine coolant heat recovery system with the exhaust only structure. It was found that the additional power recovered from the engine coolant system was 20 W out of a total 2140 W, which is around 1% improvement.

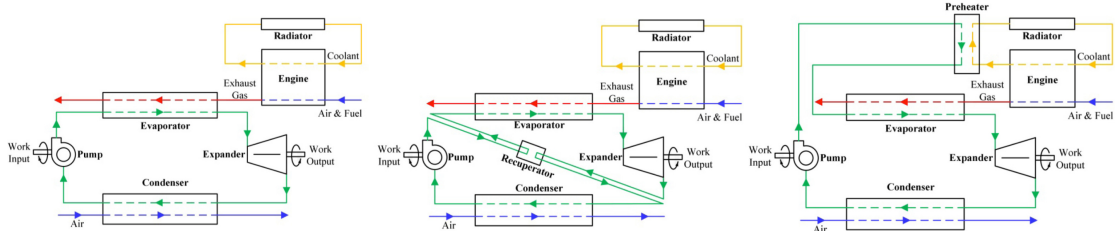


Figure 2.5: Different ORC layouts: structure 1, 2 and 3

When selecting the different configurations, different factors have to be taken into consideration as the maximization of the recovered energy is not the only objective to pursue. System complexity, component volume and weight, and the resulted extra cost added to the vehicles and the payback period are also big concerns.

2.1.3 Brayton cycle

The Brayton cycle is a thermodynamic cycle that uses a gas as a working fluid. The generalized plant configuration and the p-V and T-s diagrams are showed in Figure 2.6.

The cycle is composed by:

- **Process 1-2:** adiabatic compression, operated in a turbo-machine (compressor)
- **Process 2-3:** isobaric heat addition, operated in the combustor

- **Process 3-4:** adiabatic expansion, operated in a turbo-machine (turbine)
- **Process 4-1:** isobaric heat rejection, operated in a radiator in the case of a closed cycle

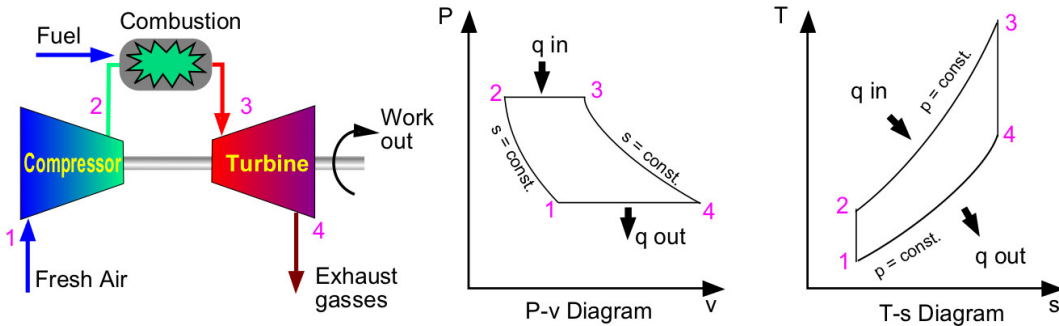


Figure 2.6: Diagrams and plant layout of an idealized Brayton cycle

The efficiency of the cycle can be calculated as:

$$\eta_t = 1 - \frac{1}{\beta^{k-1}} \quad (2.2)$$

The regular Brayton thermodynamic cycle proved itself not to be suited for a bottoming cycle type of application. Of particular importance for waste heat recovery applications is the *Super-critical CO₂* (sCO₂) Brayton cycle. Researchers claim [28] that an sCO₂ power cycle could potentially exhibit a higher thermal efficiency than steam cycles when operating between the same maximum and minimum cycle temperatures. In addition, the high energy density of sCO₂ suggests that the size requirements for the turbomachinery used in an sCO₂ power cycle could potentially be much lower than those used in steam cycle generation, which may result in lower capital costs. To date, most research in the field has been dedicated to the use of sCO₂ as the primary power cycle in nuclear applications, but relatively little research has been aimed toward developing an sCO₂ cycle that is well-suited to bottoming cycle applications.

2.1.4 Selection of the bottoming cycle

After having introduced the three most common thermodynamic cycles that can be employed as bottoming cycle, it's necessary to understand the up and downsides of the three in order to select the better one for the use case considered in this thesis.

The choice between the two different Rankine Cycles is basically reduced to the selection of the most appropriate working fluid. The choice of the working fluid to be used in the cycle depends on a number of factors, e.g. thermodynamic efficiency, environmental protection, safety, process-related and economic issues.

The steam Rankine cycle is the most reliable and simple configuration considered, it has a high efficiency due to the very small work required for the pump. Water

is widely available, cheap and does not present any issue in form of toxicity or environmental harm potential. The biggest downside of the selection of water is the huge latent heat of vaporization. According to Arias et al. [15], water is not suited to recover heat when used as a working fluid because of the mismatch between the low temperature of engine coolant and high boiling temperature of water. Water has been used in the first generation of BMW's Rankine system [18], the *Turbosteamer*, to harvest energy from exhaust gases, while ethanol was used in a separate loop for engine coolant waste heat recovery. In the second generation Turbosteamer [22], water is only heated by the exhaust gases. This is because water works best when used for high exhaust gas temperature, from 500 °C to 800 °C. Water required also superheating to avoid turbine blade erosion, if turbine is selected as expander, but the high degree of superheating makes it less practical for the automotive application due to the variation of exhaust temperature at different load conditions. Besides, its high freezing point (0 °C) cannot meet the standard automotive working temperature range (-40 °C to 85 °C).

Organic Rankine Cycle shows a much better potential for waste heat recovery in automotive applications. The low boiling point of the organic fluid allows to recover efficiently low-grade waste heat. The dry/isentropic refrigerants are widely used in small-scale RC applications because of their good heat transfer properties, excellent thermal stability and low viscosity. They are generally non-flammable, which is a big advantage for automotive application and compatible with most materials. Under typical low temperature ambient conditions they do not freeze, which is a major concern with water. Chammas and Clodic [10] compared different organic fluids with water for RC application to hybrid vehicles, arguing that using water to recover automotive waste heat could lead to a complex system requiring large size equipment and high investment cost, which makes the study on organic working fluid necessary. Domingues et al. [26] compared R123 and R245fa with water as working fluid for vehicle RC waste heat recovery potential from exhaust gas. The study revealed the advantage of using water as working fluid to recover waste heat from exhaust gas of vehicles equipped with spark-ignition engine. However, it was also found that the heat exchanger effectiveness for R123 and R245fa is higher than that for water. Consequently, when the exhaust temperature is relatively low, organic fluids can be considered appropriate for vehicle RC application. Extensive work has also been poured in ORC + internal combustion engines combinations, leading to interesting fuel saving values.

The usage of organic fluids, such as refrigerants (i.e. R134a, R245fa, etc.) carries a few shortcomings. First, the intrinsic property of dry/isentropic fluids reduce the area of net work in the T-s diagram, which means less power output compared to wet fluid, e.g. water. Second, to reduce the cooling load of the condenser, a recuperator is usually necessary to cool the superheated vapor to saturated state, increasing the system complexity and cost. Moreover, most organic fluids have relatively low thermal instability temperatures compared to water, therefore at high temperature and pressure the system might suffer chemical decomposition and deterioration. In addition, the current generation of refrigerants has a high global warming potential, which means that their use could be limited or banned in the near future.

The super-critical CO₂ Brayton cycle combines the advantages of both steam Rankine cycle and gas turbine system. In other words, the fluid is compressed in the incompressible region, and the higher turbine inlet temperature can be utilized

with less material issues compared with the steam Rankine cycle. Therefore, the volumetric flow rate decreases as the fluid density is higher, resulting in 10 times smaller turbomachinery compared with the turbomachinery of a steam Rankine cycle [29]. In addition, researchers claim [28] that an sCO₂ cycle could potentially exhibit a higher thermal efficiency than steam cycle, when operating between the same maximum and minimum temperatures. A modeling research performed by Kimzey [28] highlighted that the Brayton cycles are well suited to operating with a heat flux producing power source, but are not well suited to a sensible heat source, such as topping cycle exhaust. This is because this cycle is not truly effective at recovering waste heat: most Brayton cycles are not self-sustaining at operating temperatures below 480 °C, a problem that revealed itself also in solar thermal plants.

Given the above reasons, in this thesis an Organic Rankine Cycle has been selected as bottoming cycle to be modeled and coupled with the 3.6L V6 petrol engine Simulink model.

2.2 Introduction to split cycle engines

In the following chapter, an introduction to the basic concept of the split-cycle engine, and of alternative methodologies for recover waste heat will be provided. In the last decades engine improvements through friction reduction and improvements in the combustion system has been the main drivers, but savings will become increasingly difficult and costly [30]. The aim of this section is to introduce a different design that has the potential to achieve better results than the conventional one in terms of both efficiency and power density. The aforementioned approaches, combined with waste heat recovery, are likely to yield a maximum system efficiency of 45-50%. Further improvements to efficiencies beyond 50% require a fundamental change to ICE cycle [31].

2.2.1 Basic principles

In a conventional Otto cycle engine, each cylinder performs four strokes per cycle: intake, compression, power, and exhaust. This means that two revolutions of the crankshaft are required for each power stroke. The split-cycle engine divides these four strokes between two paired cylinders, a concept first described by Ricardo in 1908, and further developed by Carmelo Scuderi. Scuderi developed a modified version of the split-cycle engine, and filed the first patent for the *Scuderi Split Cycle* (SSC) in 2001 [32], followed by supporting patents. The SSC concept divides the four strokes of a conventional combustion engine cycle over two paired cylinders. The first cylinder, referred to as the compressor, provides intake and compression strokes. The second cylinder, referred to as the expander, provides power and exhaust strokes. The two cylinders are connected by a crossover port through which the high pressure gas is transferred from the compressor cylinder to the expander cylinder between the compression and power strokes. The splitting of the compression and expansion strokes into separate cylinders has the potential to greatly improve the overall cycle efficiency. In Figure 2.7 [33] is reported the general plan layout for a simple split cycle engine. In blue is the compression cylinder, in yellow the crossover, and in red the combustion cylinder.

A major functional benefit of the split-cycle as an internal combustion engine is

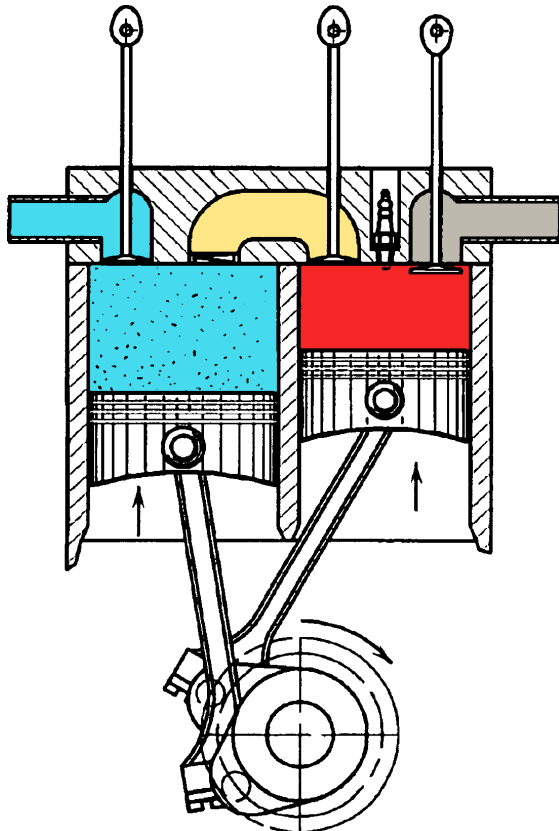


Figure 2.7: Simplest plant layout for a split cycle engine

the separation of compression and power strokes, which allows increased flexibility in optimizing these processes and designs. Other benefits are the ability for substantial Miller/Atkinson cycle type operation as extended expansion during the power stroke compared to compression stroke, or pressure charging the expander with the compressor, by use of differing compressor and expander displacements. Additionally, the crossover port arrangement enables charge motion, fuel and air mixing and combustion enhancement by means of the high pressure gas transfer from the crossover port to the expander. For SI applications, fuel injection can either be direct injection into the expander cylinder, or port injection into the crossover port during the gas transfer from the compressor into the expander (or both). Either method of injection results in less time for fuel chemical reactions leading to pre-ignition (or knock) than with intake port fuel injection used on conventional SI engines [34]. The beneficial effects of such an engine configurations are also the reduction of the compression work, due to induction into a cool cylinder or direct cooling of the charge air during compression and the possibility of high pressure waste heat recovery between the compression and combustion cylinders.

Possible losses to be minimized in a split cycle engine are the flow pumping losses past the crossover valves and through the crossover ports, and energy losses due to heat transfer from the compressed air to the crossover port walls. Since the compressor cylinder has two cooler strokes, and the power cylinder has two hotter strokes, managing thermal loading is also a challenge for split cycle engines [34].

Starting from the work of Coney et al. [35], the concept of isothermal compression has been applied to the split cycle engine to further improve its efficiency ca-

pabilities. Isothermal compression has the potential to reduce the after-compression temperature of the working fluid. By injecting the coolant media, such as liquid nitrogen or water, into the working fluid, the temperature of the compressed working fluid can be decreased significantly. It can be lower than the after-expansion temperature of the working fluid exiting the expansion cylinder. This allows to recover an increased amount of heat from the exhaust gases. This innovative methodology for waste heat recovery has been called *intra-cycle waste heat recovery* (ICWHR) [35, 31, 36]. The split cycle engine structure design allows the compression and expansion processes to happen in separate chambers, and then heat recuperation is achieved through a recuperator installed between the two chambers. Due to the isothermal compression of the charge air, the temperature difference between the compression and expansion chamber is significant, allowing an efficient recuperation.

2.2.2 Split-cycle engine operation

In the following section the principles of engine operation for the split cycle will be explained, in terms of valve timing and crank angles. The timings are referred to the Scuderi version of the engine, and are based on the work of Phillips and al. [34].

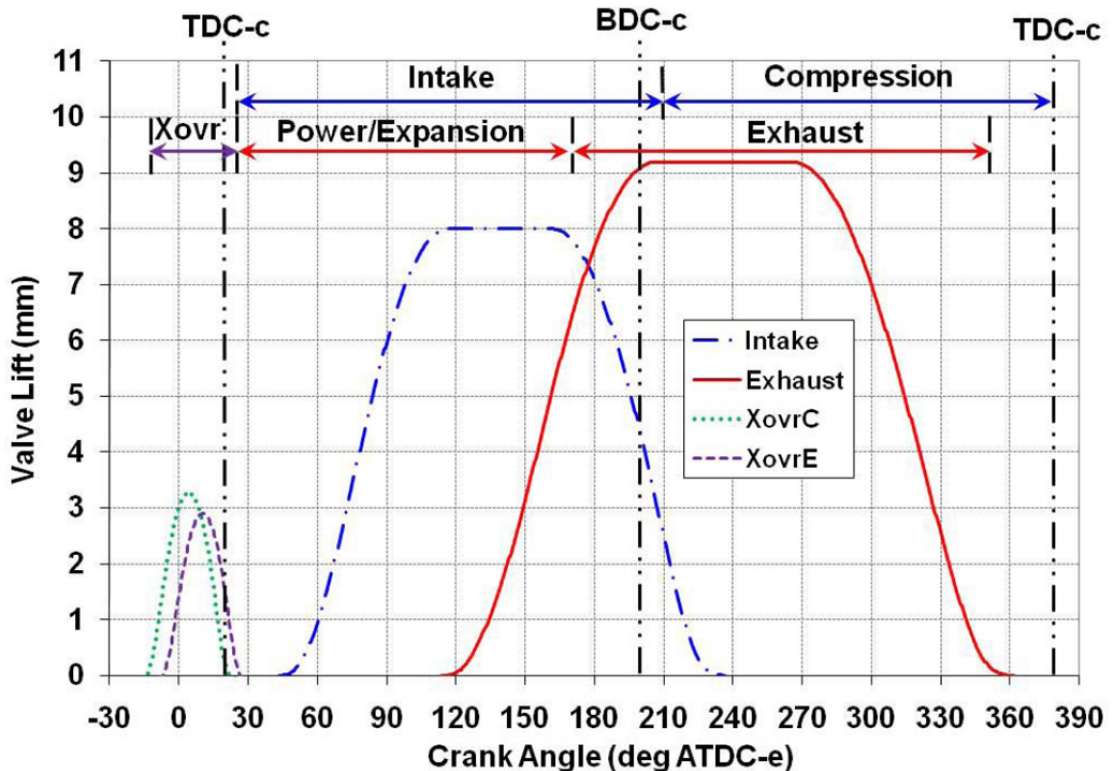


Figure2.8: Valve events for SSC engine at 4000 RPM and full load conditions

Figure2.8 shows typical valve events for the engine. The compressor top dead center (TDC) is phased 20 degrees later than the expander TDC, and thus its crank angle scale is offset 20 degrees later than the expander scale shown. The Scuderi cycle begins at intake valve opening (IVO) of the compressor. For this operating point intake valve closing (IVC) is after BDC of both cylinders. Full variable valve actuation (VVA) is needed, so that the IVC varies with speed and load, and thus early IVC is used in combination with the intake throttle to control engine mass air

flow. Compression takes place from IVC until TDC of the compressor cylinder, and overlaps the openings of the valves at the ends of the crossover (Xovr) ports, both at the compressor end (XovrC valves) as well as at the expander end (XovrE valves). In addition to the 4 phases of the conventional 4-stroke cycle, the SSC Xovr port provides a modulated high pressure gas transfer phase from compressor to expander cylinders between and overlapping the compression and power strokes. Prior to or slightly after XovrE valves open, fuel injection begins into the Xovr ports just ahead of the XovrE valves, and air and fuel mix enters the expander cylinder. As XovrE valves are nearly closed, spark ignition begins the power stroke. The power stroke ends when the exhaust valve opens (EVO) in the expander cylinder; the valve closes (EVC) just before TDC-e, ending the Scuderi cycle. Note that with fully variable intake and exhaust valve events, IVO, IVC, EVO and EVC timings can be varied with engine speed and load to optimize performance.

As the combustion takes place in an expanding cylinder, the peak temperatures are significantly lower than in a conventional engine leading to greatly reduced NOx formation. All gas-exchange and thermodynamic events are repeated every engine revolution such that the SSC can be viewed as a 4-stroke engine operating over two simultaneous 2-stroke cycles. After

2.2.3 Intra-cycle Waste Heat Recovery

In this section the advantages and some implementation aspects of ICWHR will be presented and discussed. Figure 2.9a shows the different energy fluxes that are related to an integrated waste heat recovery and to a bottoming cycle recovery.

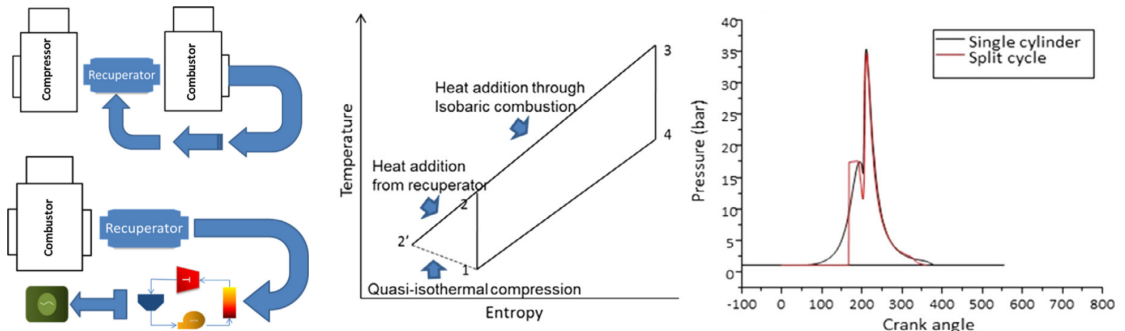


Figure 2.9: a) Comparison of the energy fluxes between an intra-cycle waste recovery and bottoming cycle type recovery, b) T-s and p-crank angle diagram for a split cycle engine with ICWHR

As shown in Figure 2.9b, the T-s diagram of the split cycle with the addition of the ICWHR is slightly different from the one showed before in Figure 2.7 due to the quasi-isothermal nature of the compression and the heat addiction coming from the recuperator.

A quasi-isothermal compression can be achieved by means of injection of water, or liquid nitrogen, during the compression phase in the first cylinder. Through the heat transfer between the intake air and the water spray droplets, the air temperature at the end of the compression stage can be decreased. The remaining liquid at the end of the compression phase can be removed using a separator.

In Figure 2.10 the layout of the engine with quasi isothermal-compression and ICWHR is shown. Ambient air (1) is pre-compressed in turbocharger, and then sent

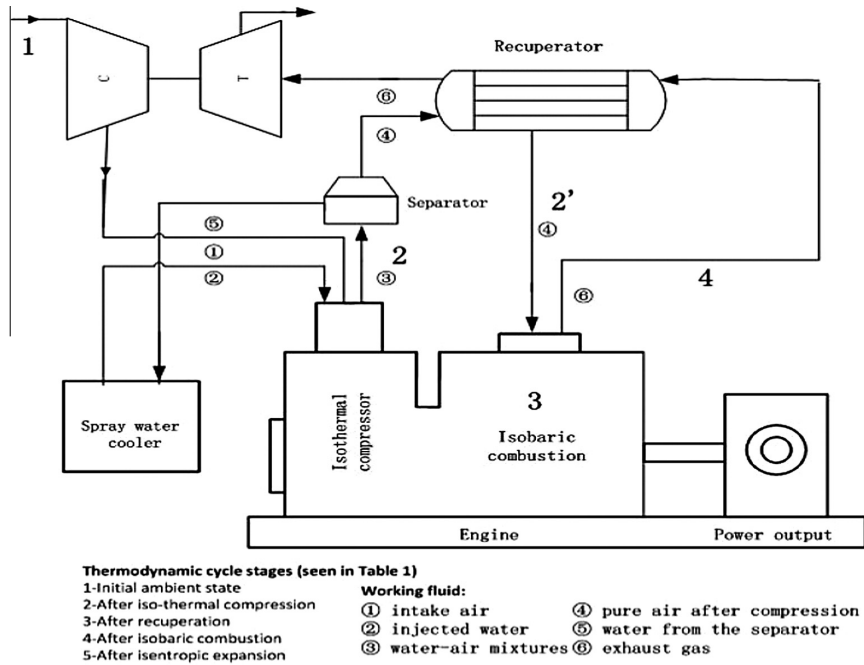


Figure 2.10: Schematic of the engine equipped with quasi-isothermal compression and ICWHR

to the reciprocating compression cylinder (2). Water is injected into the cylinder to cool down the air during compression, resulting in a quasi-isothermal compression process. After the compression stage (3), a high pressure two-phase water/air mixture leaves the isothermal compressor, and the water is recovered in a separator. The liquid water is cooled and sent back to a water tank (5). A recuperator is installed downstream the separator to heat the high-pressure air (4). Within the recuperator, the air is heated by the exhaust flow (7), and then an intra-cylinder heat recovery process is achieved. After the recuperation process (6), the fully preheated compressed air is fed to the combustion cylinders. As the combustion chamber intake valve opening time (IVO) is near to top dead centre (TDC), the diffusion of the combustion flame occurs in the expansion stroke of the cylinder. As a result, the combustion peak pressure is not increased significantly and a quasi-isobaric combustion process can be assumed. At the end of the expansion stage, the cylinder pressure is very close to the pressure in the exhaust pipe (7), so the exhaust stroke can be assumed as nearly isobaric as well. Based on the above processes, a complete split cycle is achieved [31].

CHAPTER 3 MODELING

3.1 Introduction to the model

The engine considered for this thesis work is a 3.6L V6 gasoline engine. The engine needs to be modeled in a mathematical environment in order to understand the relationships between produced work and waste heat generated, and how to develop an effective strategy to reduce the foregoing waste heat and produce additional useful power.

In this case a mathematical model for the mechanical and the thermal behavior of the engine has been developed in MATLAB/Simulink. The model is a backward-looking model, as will be explained in greater detail in Section 3.1.2. The model leverages previous models by Professor Marcello Canova and Researcher Luke DeBruin, for reduced development time.

3.1.1 Inputs and outputs

In Figure 3.1 it's shown the block diagram and conceptual schematic of the model.

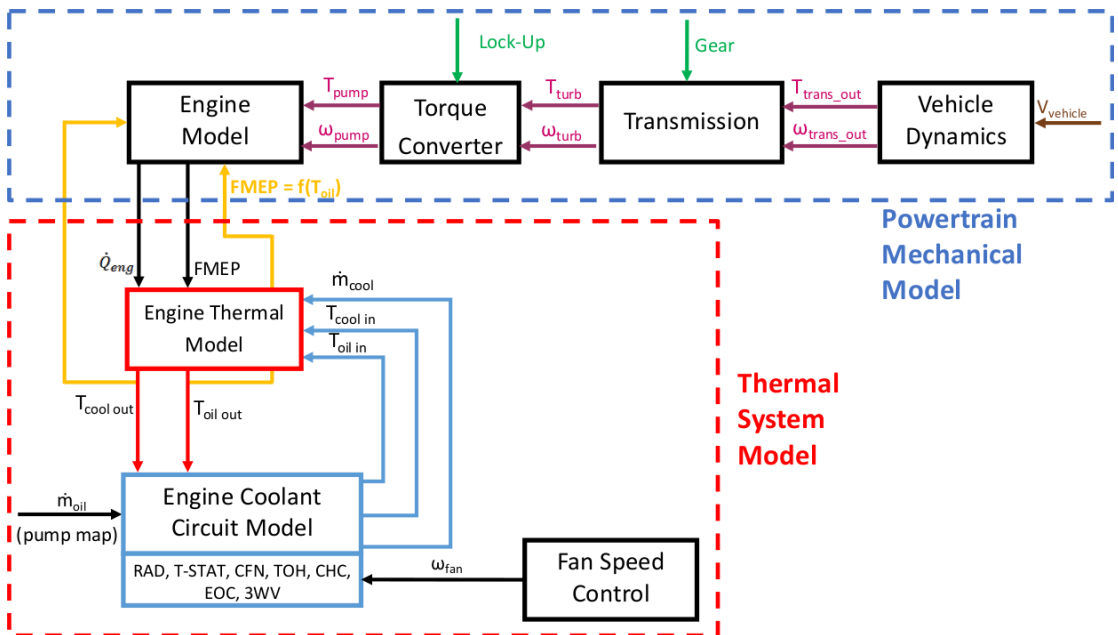


Figure 3.1: Block diagram of the model

This model is a *Backward-looking* model, that means that the torque demand is computed from the vehicle speed profile. In Forward-looking models, on the other hand, the vehicle speed is computed from the torque generated by the powertrain. A broader explanation of these two different modeling approaches will be provided in Section 3.1.2.

In Table 3.1 are shown the inputs and the desired outputs of the model, for both the mechanical and thermal part. The aim of the model is to allow the calculation of the waste heat figures for different driving conditions and engine loads. The vehicle

Inputs	Outputs
Lock-Up	Temperature coolant out from the engine block
Gear	Temperature oil out from the engine block
Vehicle speed	Temperature coolant out from the radiator Heat rejection from the radiator Rotational speed at the engine Rotational speed at the input of the transmission Fuel mass flow rate Torque at the engine Torque at the torque converter turbine Power drawn by the fan

Table3.1: Inputs and outputs of the engine model

speed is the most important input, because of the backward-looking nature of the model, and it's the starting point for the calculation of the consequent acceleration and torque. The lock-up and gear inputs allows the model to select the correct operational model for the torque converter, and the correct gear ratio in order to calculate rotational speeds in the most precise possible way. The outputs are both thermal and mechanical.

3.1.2 Forward and backward modeling approach

In general, the approach for writing a model may be of two different kinds: forward-looking or backward-looking. As said before, in a *Forward-looking* model, the vehicle speed is computed from the torque generated by the powertrain. It accounts for longitudinal vehicle dynamics and effects for crankshaft and transmission inertia, but it's necessary to model the driver behavior, as well as controls for engine, torque converter and transmission. This structure allows to have a very precise model, but may also lead to overly complex and long to develop models.

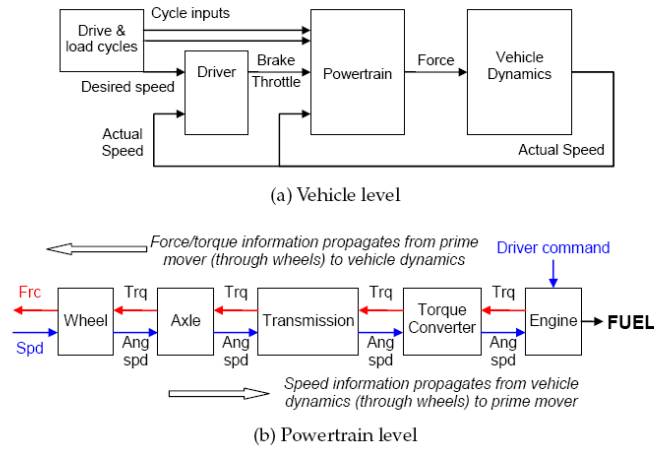
In a *Backward-looking* model, the torque demand is computed from the vehicle speed profile. In this case, the only information needed are the vehicle speed profile, the torque converter lockup and the gear shift profiles. It does not require detailed information on engine and transmission controls, and the model is quasi-static, hence vehicle longitudinal dynamics and powertrain inertia are neglected. In Figure3.2 are shown the block diagrams of the structure of a model for both approaches.

The model used in this project is Backward-looking, as the focus of the analysis is on the thermal system and not the complete powertrain. The heat rejection rates from the engine can be calculated easily from this type of model. The effect of coolant, oil and fan cooling on the drive-train efficiency can still be captured by the simulation via the adoption of engine heat rejection maps.

3.2 Equations for the mechanical behavior

The backward model requires inputs and outputs to be inverted with respect to the energy flow in the engine. In this section the equations for the mechanical behavior of the engine will be provided, while in Section3.3 the energy balance and thermal section of the model will be explained

Block Diagram of Powertrain Forward-Looking Model



Block Diagram of Powertrain Backward-Looking Model

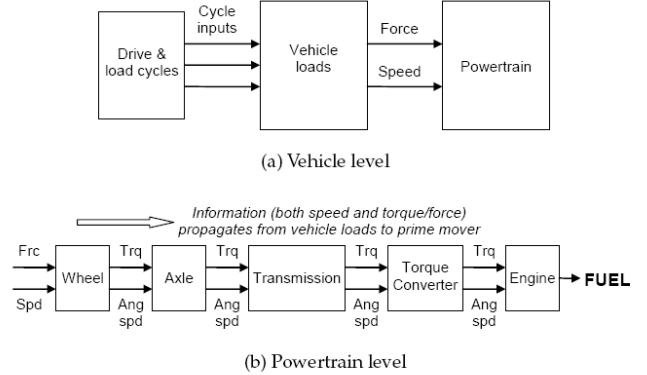


Figure 3.2: Block diagram of Powertrain Forward-Looking and Backward-Looking Model

3.2.1 Vehicle Longitudinal Dynamics Model

The vehicle speed profile is used to calculate the force at wheel, and torque demand at transmission output shaft is calculated from wheel radius and gear ratio.

The force at the wheel may be calculated as:

$$F_{wheel} = (M + M_{eq}) \frac{dV_{veh}}{dt} + F_{aero} + F_{rolling} + F_{grade} \quad (3.1)$$

with the different forces expressed as:

$$\begin{aligned} F_{aero} &= C_s \rho_{air} \Omega \frac{V_{veh}^2}{2} \\ F_{rolling} &= C_g M g \cos(\Theta) \\ F_{grade} &= 0 \end{aligned}$$

allows the calculation of the output torque

$$T_{output} = \frac{F_{wheel}}{R_{wheel} \tau_{diff}} \quad (3.2)$$

3.2.2 Transmission model

Input speed and input torque are computed starting from speed and torque demand at output shaft.

$$T_{input} = \frac{T_{output}}{\eta(T_{output}, \omega_{output}) \theta(gear)} \quad (3.3)$$

$$\omega_{input} = \tau(gear) \omega_{output} \quad (3.4)$$

3.2.3 Torque converter model

To calculate pump speed and torque, the ones relative to the turbine are needed. The Speed ratio may be defined as a function of the turbine speed.

$$\omega_p = \frac{\omega_t}{SR}$$

$$T_p = \frac{T_t}{TR}$$

$$Q_{TC} = \omega_p T_p - \omega_t T_t$$

Regarding the conditions of unlocked torque converter, it's needed to define maps for Speed Ratio and for Torque Ratio. In Figure3.3 are shown the maps used in the model, extrapolated from experimental data.

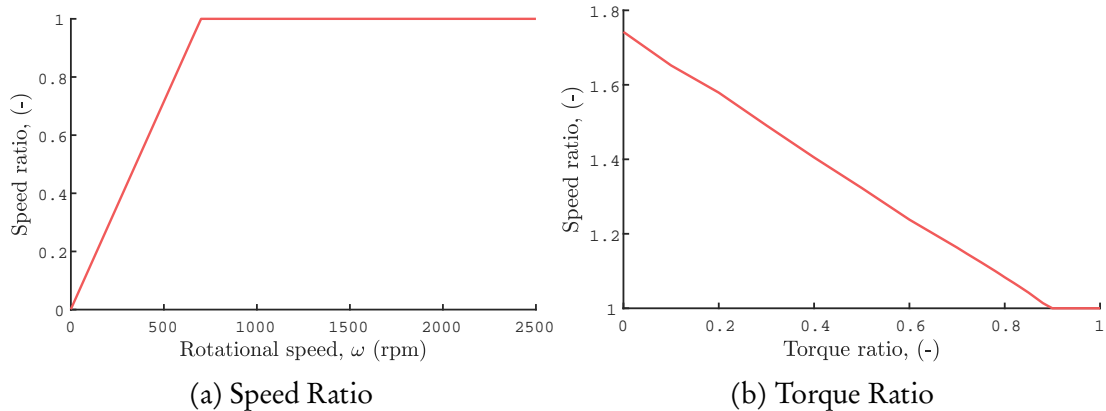


Figure3.3: Maps for the unlocked torque converter

3.3 Energy balance

This part of the model represents a simplified Thermal Management System (TMS) of a typical automotive engine. In Figure3.4 the structure of the model is shown.

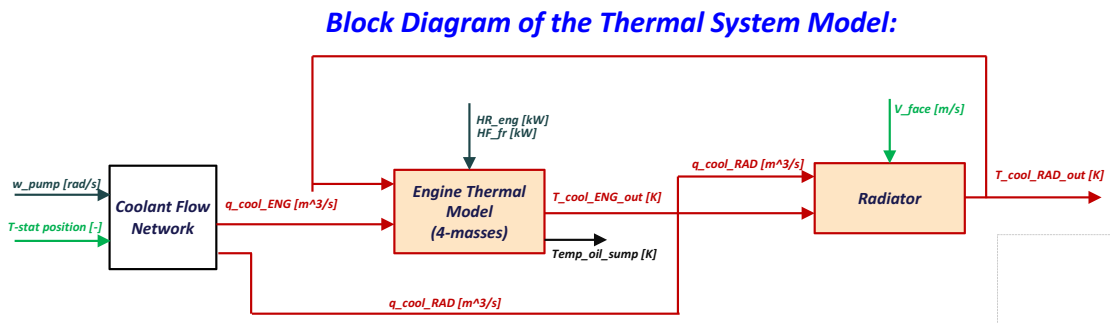


Figure3.4: Block diagram of the thermal system model

This is an engine transient model whose objective is to predict the dynamics of the coolant temperature during warmed conditions, assisting in the design of cooling and oil system thermal control.

3.3.1 Thermal model

The engine thermal model consists of a lumped parameters thermal mass model that predicts the thermal dynamics of the engine, based on the work of Scott and al. [37]. Because of the significant differences between coolant and oil temperatures during engine warm up and their effects on engine friction and coolant temperature, more than one mass is needed. The number of mass selected is three: block, crank, and sump. The *block* contains all the coolant passages and, assuming well mixed coolant, the coolant outlet temperature equals the block average temperature. The *crank* consists of the crankshaft, pistons, connecting rods, main bearings, and supporting structure. The *sump* is the oil reservoir and oil pan structure. In Figure 3.5 the three masses are shown. The division between the block and the crank is taken at the bottom of the coolant passages. Thus there is both oil and coolant flow to the block but no coolant flow in the crank. The crank-sump division is at the oil pan gasket.

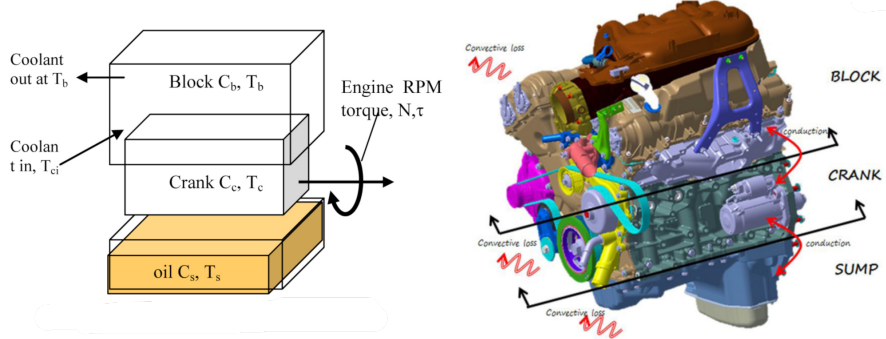


Figure 3.5: Three mass engine model and general engine division into parts

In Figure 3.5 are shown the energy flows in the engine, according to [37]. The dotted line represents the boundary used to define the system for the steady state energy balance used in evaluating heat loss to coolant, oil, and convection/radiation. For the engine as a whole, energy enters with fuel and air and leaves with the exhaust gas, brake power, and heat rejected to coolant, oil, and surrounding ambient. At steady state, the energy flows must balance.

The gross indicated mechanical power released by the combustion process minus the pumping work is the net indicated mechanical power that acts on the piston face, shown as \dot{W}_{ni} in the diagram. The pumping work is converted to heat and, plus the heat from the combustion, is transferred to the cylinder walls, head, and piston. The heat energy that enters the engine can be calculated from the energy balance on the combustion chamber.

$$\dot{Q}_{heat} = \dot{E}_{air} + \dot{E}_{fuel} - \dot{E}_{ex} - \dot{W}_{ni} \quad (3.5)$$

The friction power may be determined, if direct measures of indicated power and pumping work are available, as:

$$\dot{W}_f = \dot{W}_{ni} - \dot{W}_b \quad (3.6)$$

Q_{heat} and W_f may be determined from steady state tests on the engine. Correlating them with engine operating parameters, for any required brake power and RPM it's possible to find Q_{heat} and W_f for use.

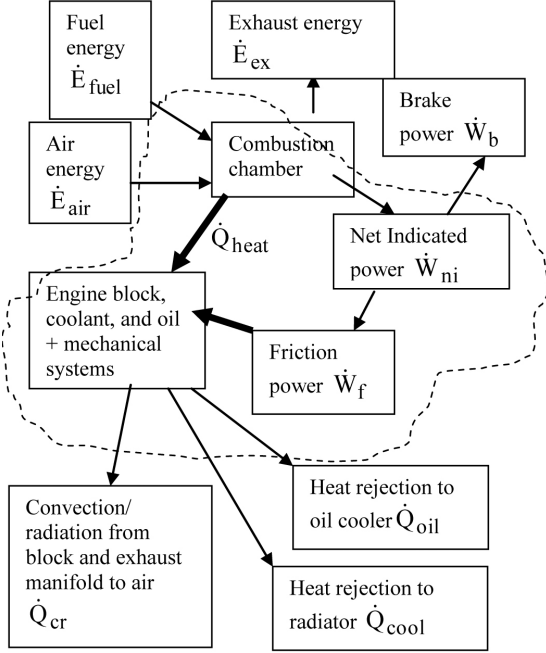


Figure 3.6: Energy flows in the engines

The energy flows needs thus to divided among the three thermal masses. The friction work may be divided between the crank, which includes the pistons, and the block, which includes the valve train. f_v can be defined as the fraction of the total friction work that is assigned to the block mass. The heat leaving the combustion process goes to the block and the piston, then it's possible to define f_h as the fraction of Q_{heat} that goes to the block.

The energy transfers between the block, crank, and sump take place through the conduction paths and the oil flow. The conduction between the masses is considered to be a linear function of the temperature differences, using an overall heat transfer coefficient UA_{bc} between the block and the crank, and UA_{cs} between the crank and the sump. Each mass has some thermal capacity C equal to mass times specific heat.

The transient heat equations for the three engine thermal maps are now shown:
BLOCK MASS

$$C_b \frac{dT_b}{dt} = f_h \dot{Q}_{heat} + f_v \dot{W}_f - f_b \dot{m}_o c_{po} [T_b - T_c] - UA_{bc} [T_b - T_c] - UA_{ba} [T_b - T_a] - \dot{m}_c c_{pc} [T_b - T_{ci}] \quad (3.7)$$

CRANK MASS

$$C_c \frac{dT_c}{dt} = [1 - f_h] \dot{Q}_{heat} + [1 - f_v] \dot{W}_f + UA_{bc} [T_b - T_c] - f_b \dot{m}_o c_{cpo} [T_c - T_b] + \dot{m}_o c_{po} [T_s - T_c] - UA_{cs} [T_c - T_s] - UA_{ca} [T_c - T_a] \quad (3.8)$$

SUMP MASS

$$C_s \frac{dT_s}{dt} = \dot{m}_o c_{po} [T_c - T_s] + UA_{cs} [T_c - T_s] - UA_{sa} [T_s - T_a] \quad (3.9)$$

3.3.2 Radiator model

The radiator has a relatively slow response, due to the large thermal mass. The model is based on a paper by Scott and al.[38], and it's a simplified version of the multi-node thermal model. Only one node is considered, and three different energy balance equations has to be defined.

Energy Balance for COOLANT CONTROL VOLUME

$$C_c \frac{dT_c}{dt} = \dot{m}_c c_{p,c} (T_{c,in} - T_c) - A_f \frac{C_f \dot{m}_c^\beta}{C_3} (T_c - T_w) \quad (3.10)$$

Energy balance for WALL THERMAL MASS

$$C_w \frac{dT_w}{dt} = A_f \frac{C_f \dot{m}_c^\beta}{C_3} (T_c - T_w) - A_f \frac{1}{C_2} (T_w - T_s) \quad (3.11)$$

Energy balance for FINS AND EXTERNAL SURFACE IN CONTACT WITH AIR

$$C_w \frac{dT_s}{dt} = A_f \frac{1}{C_2} (T_w - T_s) - A_f \frac{(\rho_{air} V_{face})^{\frac{2}{3}}}{C_1} (T_s - T_{air}) \quad (3.12)$$

In steady-state conditions, the heat transfer through the radiator assumes the simplified formulation

$$\begin{aligned} \dot{Q} &= A_f \frac{C_f \dot{m}_c^\beta}{C_3} (T_c - T_w) \\ &= A_f \frac{1}{C_2} (T_w - T_s) \\ &= A_f \frac{(\rho_{air} V_{face})^{\frac{2}{3}}}{C_1} (T_s - T_{air}) \end{aligned} \quad (3.13)$$

3.3.3 Coolant flow and engine heat rejection model

The mass flow rates of the cooling fluid and engine oil must be computed, order to appear in the energy balance equation. Maps extrapolated from experimental data and lookup tables allows the calculations. In Figure?? are shown the maps used.

[INSERIRE MAPPE]

3.4 Results

In this sections the results of the model will be presented and explained. Two different drive-cycles have been used to test the model in different conditions and on different use cases. The drive-cycles considered are the *New European Drive Cycle* (NEDC), which is supposed to represent the typical usage of a car in Europe, and *Federal Test Procedure 75* (FTP-75), which is a test procedure defined by the US Environmental protection agency and more representative of US car usage. The standard speed profiles for both drive cycles are shown in Figure3.7

As explained in Section3.1.2, being the model Backward-looking, the gear shifting data and lockup status for the torque converter must be provided from direct

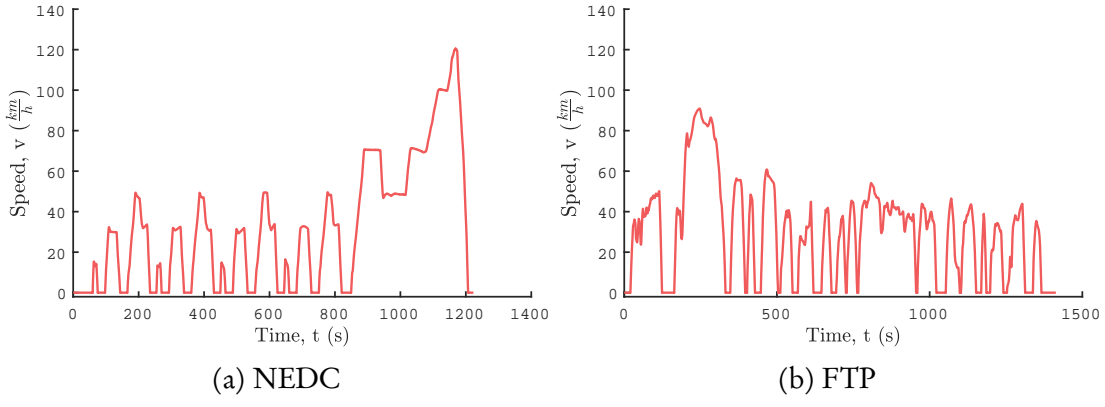


Figure 3.7: Speed profiles of the considered drivecycles

measurements on the vehicle. Figure 3.8 shows the aforementioned data needed for running the simulation.

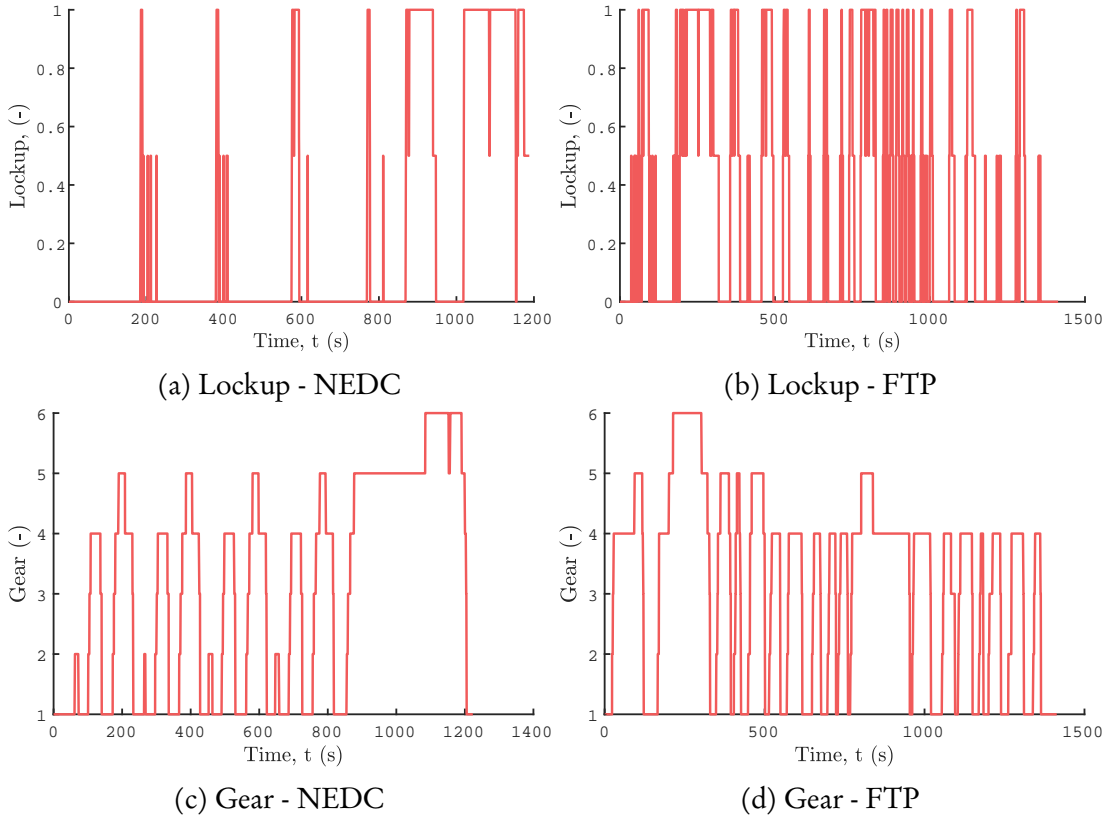


Figure 3.8: Lockup and gear profiles

Being this model focused on the fuel consumption and energetic measures, a good method for understanding the accuracy of the simulation is the calculation of the integral as area under the curve relative to mass flow rate of fuel as shown in Figure 3.12. The value calculated starting from the experimental values is 1.1114 kg, while the simulated one is 1.0601 kg for the FTP cycle. Regarding the NEDC, values are 0.9333 kg for experimental, and 0.9651 kg for simulated. The error is 4.61% and 3.41% respectively, which is acceptable for a backward-looking model.

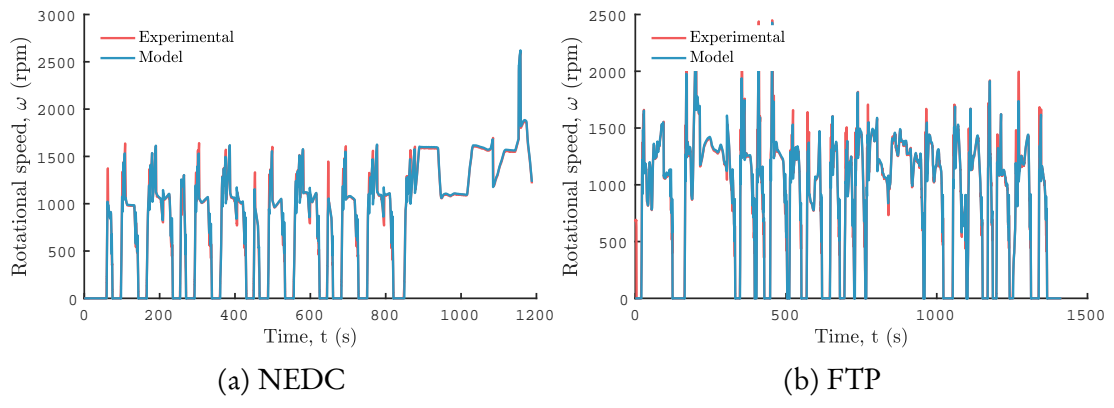


Figure3.9: Rotational speed at transmission input

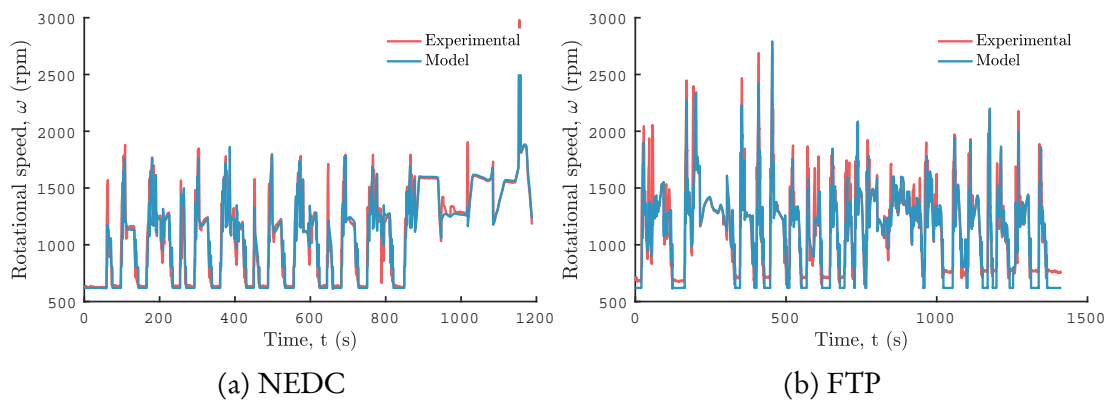


Figure3.10: Rotational speed at the engine

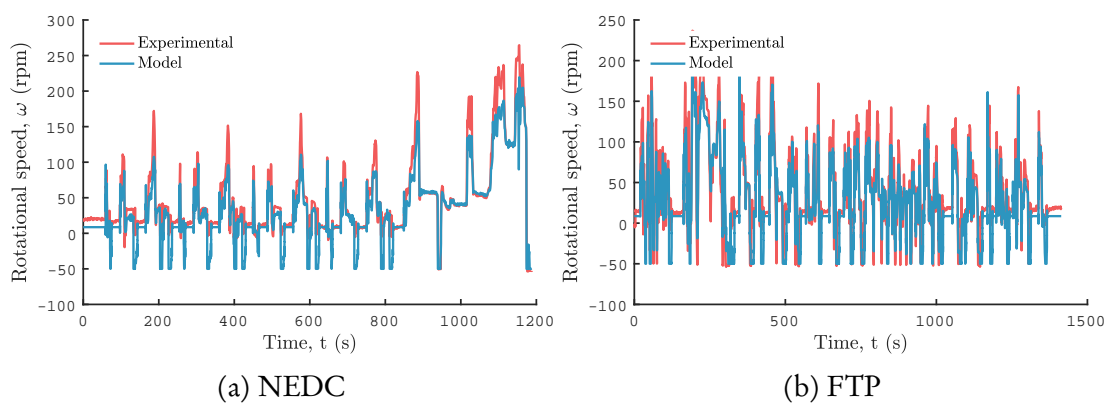


Figure3.11: Engine torque

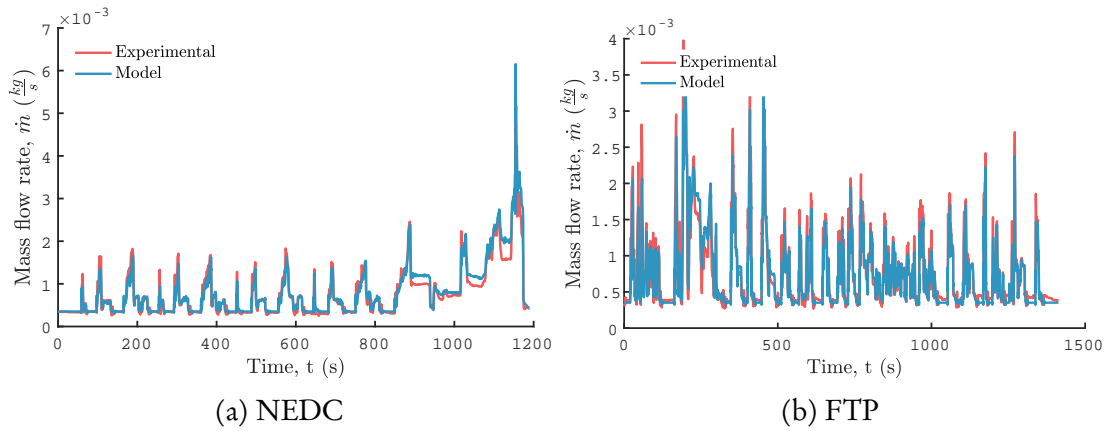


Figure3.12: Fuel mass flow rate

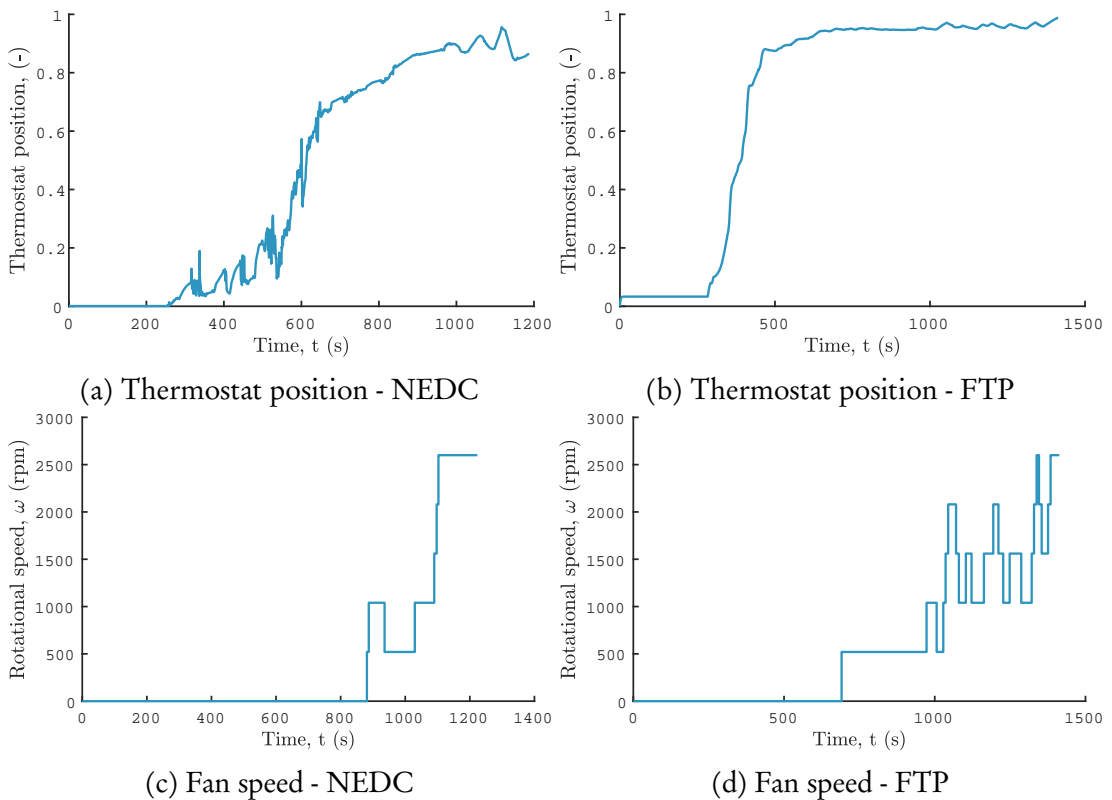
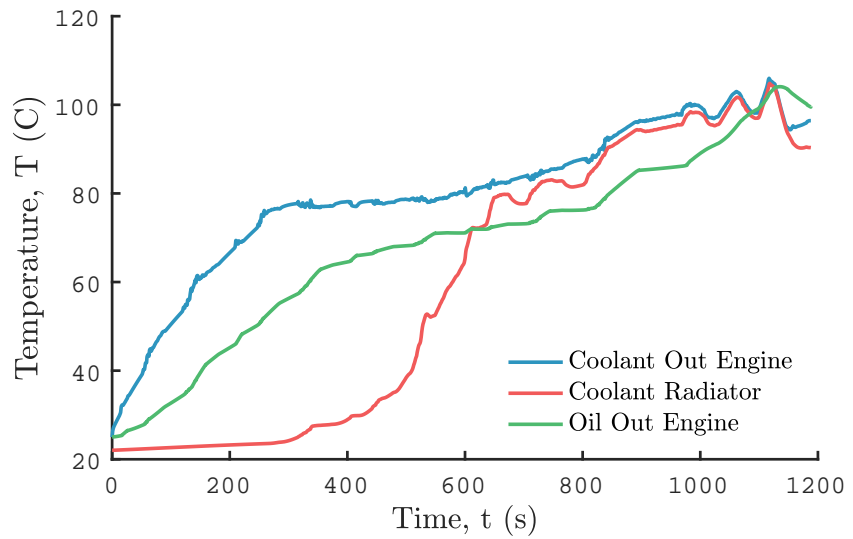
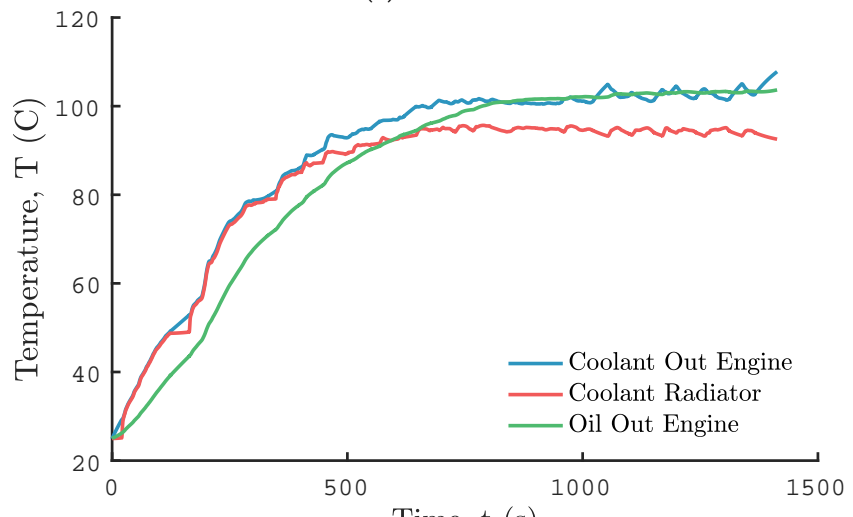


Figure3.13: Thermostat position and fan speed



(a) NEDC



(b) FTP

Figure 3.14: Temperatures of engine fluids

REFERENCES

- [1] IPCC, *Climate Change 2014: Mitigation of Climate Change*. 2014, p. 1454, isbn: 9781107654815. arXiv: arXiv:1011.1669v3.
- [2] N. GISS, *Global mean estimates based on land and ocean data*, 2016.
- [3] N. Unger, T. C. Bond, J. S. Wang, D. M. Koch, S. Menon, D. T. Shindell, and S. Bauer, “Attribution of climate forcing to economic sectors.,” *Proceedings of the National Academy of Sciences of the United States of America*, vol. 107, no. 8, pp. 3382–7, 2010.
- [4] Bureau of Transportation Statistics, *Average fuel efficiency of u.s. light duty vehicles*, 2016.
- [5] ——, *Safety, energy, and environmental impacts of passenger travel*, 2016.
- [6] United States Environmental Protection Agency, “Light-duty automotive technology, carbon dioxide emissions, and fuel economy trends: 1975 through 2016,” no. November, 2016.
- [7] J. D. Miller and C. Facanha, “The state of clean transport policy - a 2014 synthesis of vehicle and fuel policy developments,” p. 73, 2014.
- [8] Transportpolicy.net, *Global comparison: light-duty emissions*, 2016.
- [9] A. Boretti, “Recovery of exhaust and coolant heat with r245fa organic rankine cycles in a hybrid passenger car with a naturally aspirated gasoline engine,” *Applied Thermal Engineering*, vol. 36, no. 1, pp. 73–77, 2012.
- [10] R. El Chammas and D. Clodic, “Combined cycle for hybrid vehicles,” 2005.
- [11] J. C. Conklin and J. P. Szybist, “A highly efficient six-stroke internal combustion engine cycle with water injection for in-cylinder exhaust heat recovery,” *Energy*, vol. 35, no. 4, pp. 1658–1664, 2010.
- [12] V Dolz, R Novella, A Garcia, and J Sanchez, “Hd diesel engine equipped with a bottoming rankine cycle as a waste heat recovery system. part 1: study and analysis of the waste heat energy,” *Applied Thermal Engineering*, Vol 36, pp 269–278, 2012.
- [13] T. Wang, Y. Zhang, J. Zhang, G. Shu, and Z. Peng, “Analysis of recoverable exhaust energy from a light-duty gasoline engine,” *Applied Thermal Engineering*, vol. 53, no. 2, pp. 414–419, 2013.
- [14] H. Oomori and S. Ogino, “Waste heat recovery of passenger car using a combination of rankine bottoming cycle and evaporative engine cooling system,” 1993.
- [15] D Arias, T Shedd, and R Jester, “Theoretical analysis of waste heat recovery from an internal combustion engine in a hybrid vehicle,” *SAE World Congress & Exhibition: Thermal Systems and Climate*, no. 724, 2006.
- [16] T. Endo, S. Kawajiri, Y. Kojima, K. Takahashi, T. Baba, S. Ibaraki, T. Takahashi, and M. Shinohara, “Study on maximizing exergy in automotive engines,” 2007.

- [17] M. Kadota and K. Yamamoto, “Advanced transient simulation on hybrid vehicle using rankine cycle system,” *SAE International Journal of Engines*, vol. 1, no. 1, pp. 2008–01–0310, 2008.
- [18] R. Freymann, W. Strobl, and A. Obieglo, “The turbosteamer: a system introducing the principle of cogeneration in automotive applications,” *MTZ worldwide*, vol. 69, no. 5, pp. 20–27, 2008.
- [19] A. Duparchy, P. Leduc, G. Bourhis, and C. Ternel, “Heat recovery for next generation of hybrid vehicles: simulation and design of a rankine cycle system,” *World Electric Vehicle Journal*, vol. 3, no. 1, pp. 440–456, 2009.
- [20] M. He, X. Zhang, K. Zeng, and K. Gao, “A combined thermodynamic cycle used for waste heat recovery of internal combustion engine,” 2011.
- [21] X. ZHANG, K. ZENG, S. BAI, Y. ZHANG, and M. HE, “Exhaust recovery of vehicle gasoline engine based on organic rankine cycle,” 2011.
- [22] R. Freymann, J. Ringler, M. Seifert, and T. Horst, “The second generation turbosteamer,” *MTZ worldwide*, vol. 73, no. 2, pp. 18–23, 2012.
- [23] T. A. Horst, W. Tegethoff, P. Eilts, and J. Koehler, “Prediction of dynamic rankine cycle waste heat recovery performance and fuel saving potential in passenger car applications considering interactions with vehicles’ energy management,”
- [24] A. A. Boretti, “Transient operation of internal combustion engines with rankine waste heat recovery systems,” *Applied Thermal Engineering*, vol. 48, pp. 18–23, 2012.
- [25] E. Wang, Z. Yu, C. Peter, Z. Hongguang, Y. Fubin, and C. Bei, “Thermodynamic analysis of a dual-loop organic rankine cycle (orc) for waste heat recovery of a petrol engine.,” *Heat Powered Cycles Conference 2016*, no. August, pp. 27–29, 2016.
- [26] A. Domingues, H. Santos, and M. Costa, “Analysis of vehicle exhaust waste heat recovery potential using a rankine cycle,” 2012.
- [27] I. Vaja and A. Gambarotta, “Internal combustion engine (ice) bottoming with organic rankine cycles (orcs),” *Energy*, vol. 35, no. 2, pp. 1084–1093, 2010.
- [28] G. Kimzey, “Development of a brayton bottoming cycle using supercritical carbon dioxide as the working fluid,” *EPRI Report*, pp. 1–31, 2012.
- [29] Y. Ahn, S. J. Bae, M. Kim, S. K. Cho, S. Baik, J. I. Lee, and J. E. Cha, “Review of supercritical co₂ power cycle technology and current status of research and development,” *Nuclear Engineering and Technology*, vol. 47, no. 6, pp. 647–661, 2015.
- [30] D. W. Stanton, “Systematic development of highly efficient and clean engines to meet future commercial vehicle greenhouse gas regulations,” *SAE International Journal of Engines*, vol. 6, no. 3, pp. 2013–01–2421, 2013.
- [31] G. Dong, R. Morgan, and M. Heikal, “A novel split cycle internal combustion engine with integral waste heat recovery,” *Applied Energy*, vol. 157, pp. 744–753, 2015.
- [32] C. J. Scuder, “Split four stroke cycle internal combustion engine,” vol. 2, no. 12, 2003.

- [33] R Gentili, R Rossi, and E Musu, *Split-cycle engine*, 2014.
- [34] F. Phillips, I. Gilbert, J.-P. Pirault, and M. Megel, “Scuderi split cycle research engine: overview, architecture and operation,” *SAE Technical Paper*, vol. 4, no. 2011-01-0403, pp. 450–466, 2011.
- [35] M. W. Coney, C. Linnemann, and H. S. Abdallah, “A thermodynamic analysis of a novel high efficiency reciprocating internal combustion engine - the isoengine,” *Energy*, vol. 29, no. 12-15 SPEC. ISS. Pp. 2585–2600, 2004.
- [36] R. Morgan, G. Dong, A. Panesar, and M. Heikal, “A comparative study between a rankine cycle and a novel intra-cycle based waste heat recovery concepts applied to an internal combustion engine,” *Applied Energy*, vol. 174, pp. 108–117, 2016.
- [37] T. C. Scott, F.-L. Chang, M. Khandaker, and S. Uppuluri, “Transient thermal modeling of power train components,” *SAE International Journal of Passenger Cars - Mechanical Systems*, vol. 5, no. 2, pp. 2012-01-0956, 2012.
- [38] T. C. Scott, “Modeling compact exchangers for hvac applications,” in *Heat Transfer: Volume 1*, ASME, 2003, pp. 629–636, isbn: 0-7918-3693-2.